PHILOSOPHICAL TRANSACTIONS OF THE ROYAL SOCIETY A MATHEMATICAL, PHYSICAL & ENGINEERING SCIENCES

The Pyroclastic Deposits of the 1875 Eruption of Askja, Iceland

R. S. J. Sparks, L. Wilson and H. Sigurdsson

Phil. Trans. R. Soc. Lond. A 1981 **299**, 241-273
doi: 10.1098/rsta.1981.0023

THE PYROCLASTIC DEPOSITS OF THE 1875 ERUPTION OF ASKJA, ICELAND

By R. S. J. SPARKS†, L. WILSON‡ AND H. SIGURDSSON§

† *Department of Earth Sciences, University of Cambridge, Downing Place, Cambridge CB2 3EW, U.K.*

‡ *Environmental Science Department, Lancaster University, Lancaster LA1 4TQ, U.K.*

§ *Graduate School of Oceanography, University of Rhode Island, Kingston, RI 02881, U.S.A.*

(*Communicated by G. P. L. Walker, F.R.S. – Received 4 September* 1979)

[Plates 1–4]

CONTENTS

The 1875 explosive eruption of Askja, Iceland was part of a series of regional volcanic and tectonic events which took place in the northern rift zone in 1874 and 1875. These events were marked by regional seismicity, graben formation and a basaltic fissure eruption at Sveinagja, and the plinian eruption of Askja on 28–29 March. Crustal rifting caused basaltic magma to be mixed with rhyolitic magma, triggering the plinian eruption. A caldera, Oskjuvatn, was formed in Askja measuring 3 × 4 km and 267 m deep. Six distinguishable pyroclastic layers can be recognized. The main eruption began with a small sub-plinian pumice eruption forming layer B. The next phase produced a fine-grained, poorly sorted pumice and ash deposit with well developed stratification (layer C), which contains base surge beds near source and is interpreted as phreatomagmatic in origin. The main plinian phase of the eruption lasted 6 h and formed a coarse-grained, poorly bedded pumice-fall deposit (layer D) which contains 75% of the total ejecta. Late-stage explosions formed a layer of lithic clasts (layer E). Isopach and grain-size isopleth maps show that the vents migrated from south to north along a line 1.5 km long in the area now occupied by Oskjuvatn. The intensity and column height of the eruption increased with time as shown by reverse grading and an increasing dispersal index in successive layers. Most of the ejecta is composed of white rhyolitic pumice and ash. Lithics consist of rhyolitic obsidian, partially fused trondhjeimite, and basalt fragments: layer D contains 2.1 mass % lithics. All layers

contain abundant grey pumice clasts consisting of intimate mixtures of dark brown basaltic and brown rhyolitic glasses. The mass percentage of mixed pumice in layer D is 4.7, of which 40 % is basaltic glass. These mixed pumice clasts are concentrated at distances of 30–80 km in layer D by æolian sorting. A grey, crystal-rich, andesitic pumice occurs as inclusions in the white pumice. Layer D shows a systematic decrease in median grain diameter, but no change in σ_ϕ with distance from source. Layer C shows no change in median grain diameter, but a decrease in σ_ϕ with distance from source. Phreatomagmatic deposits such as layer C can be readily distinguished from plinian deposits on a Md_ϕ against σ_ϕ diagram, on a σ_ϕ against α_ϕ (skewness) diagram and on the F against D plot of Walker (1973). The downwind, coarse-tail grading in layer C is attributed to fall-out of fine ash as clumps and aggregates. The total grain-size distributions of both layers D and C show bimodality. In layer D a minor mode in the ash size classes reflects secondary processes of fragmentation by collisions in the vent and column, whereas the major mode is due to disruption of magma by expanding gases. In layer C the fine mode is dominant and represents extensive fragmentation by explosive interaction with water. Field and grain-size studies of layer D show that impact breakage is of major importance near source.

Introduction

The paroxysmal plinian eruption of Askja on 28–29 March 1875 was one of the major explosive rhyolitic eruptions to have taken place in post-glacial times in Iceland. There is abundant historical evidence on the eruption (Thoroddsen 1925), and the studies of Thorarinsson (1934, 1963, 1968, 1971) make it one of the most carefully studied plinian air-fall deposits. The good preservation of the deposit provides a favourable opportunity to investigate the mechanisms of plinian volcanism.

Our study divides the deposit into several distinguishable layers which represent discrete phases and styles of activity. Studies of layer thickness, grain size variations, ejecta density and ejecta lithologies constitute the principal field observations, largely by means of methods developed by Thorarinsson (1944, 1971), Walker & Croasdale (1971) and Suzuki *et al.* (1973) which provide a framework for volcanological and petrological studies of the ejecta and for modelling the eruption. Our interpretations of the eruption and its products rely considerably on contemporaneous observations and we therefore present a detailed account of the historical evidence.

The youth and good preservation of the pyroclastic deposits permitted a comprehensive study of the lateral and vertical changes in grain size and texture, which can be interpreted in terms of changing style and intensity of the eruption. We estimate the total grain-size population of each layer, which provides essential data for understanding fundamental processes of explosive volcanism. We also evaluate grain-size measurement techniques which have been previously developed on less well preserved prehistoric pyroclastic deposits. Askja provides an opportunity to characterize a plinian deposit for which some of the circumstances of eruption are already known, and others can be constrained with unusual precision.

Geological background

The Askja massif is the largest of several central volcanoes located in the northeastern rift zone of Iceland (figure 1). The recent activity at Krafla (Bjornsson *et al.* 1977, 1979) coupled with the geological studies of quaternary and tertiary central volcanoes (Saemundsson 1974;

Walker 1975) have elucidated the broad behaviour of central volcanoes. Each central volcano appears to be a focus of basalt volcanism with the output and frequency of volcanism being significantly greater than in the surrounding lava plains. Each volcano is characterized by a central fissure swarm which is preserved as a dyke swarm in the dissected tertiary centres (Walker 1960, 1975). These volcanoes commonly have one or more caldera, and are associated with acid magnatism. During periods of regional crustal rifting central volcanoes become activated (Bjornsson *et al.* 1979; Sigurdsson & Sparks 1978*a*).

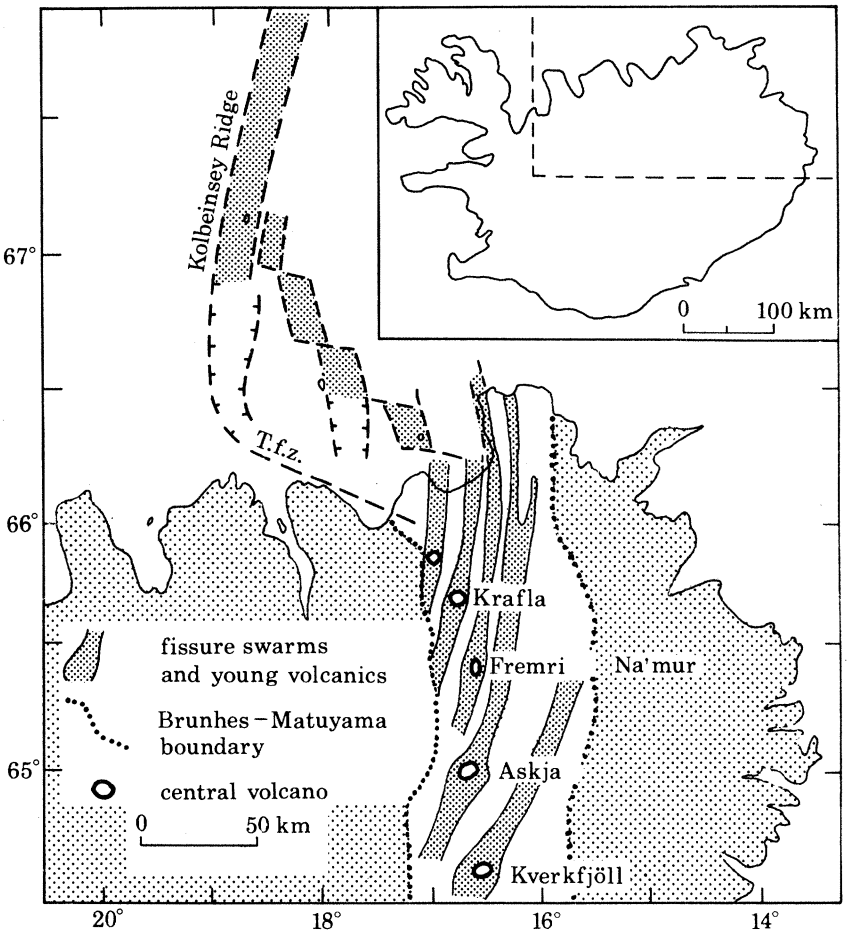

FIGURE 1. Location of central volcanoes and their associated fissure swarms in the northeastern volcanic zone of Iceland. T.f.z., Tjornes fracture zone.

Askja (figure 2, figure 3 (plate 1), figure 4) shows all the essential features of a central volcano. The main massif is composed of a sub-glacial palagonite formation which delineates a broad ring (Sigvaldason 1964, 1968). The prehistoric Askja caldera (8 km diameter) forms a central depression (figures 3 and 4). Sigvaldason (1968) has recognized a number of distinctive units within the palagonite massif, and that many subglacial eruptions have apparently contributed to its construction. In post-glacial times the large Askja caldera has been filled by a large volume of basaltic lava, with some vents located on the caldera ring fracture. Historical records only go back to the 1874–75 events, which were manifestations of a regional rifting episode in the northern part of the eastern volcanic zone. Contemporaneous basalt fissure eruptions at Sveinagja, 70 km north of Askja, in 1875 are now linked with the rhyolitic eruption as parts of

the same volcanic–tectonic event (Sigurdsson & Sparks 1978*b*) involving the rifting of a high-level magma reservoir beneath Askja. Small basalt eruptions occurred in 1921–26 at four centres located around the Oskjuvatn caldera which formed after the 1875 eruption (Sigvaldason 1964; Thorarinsson 1968). There was also a larger-volume fissure eruption in 1930 on the south flanks (figures 2 and 3). In October 1961 a basaltic eruption took place on the northeast rim of the main Askja caldera producing 11 km² of lava (Thorarinsson 1963, 1968). Acid magma in Askja is only represented by the products of the 1875 eruption.

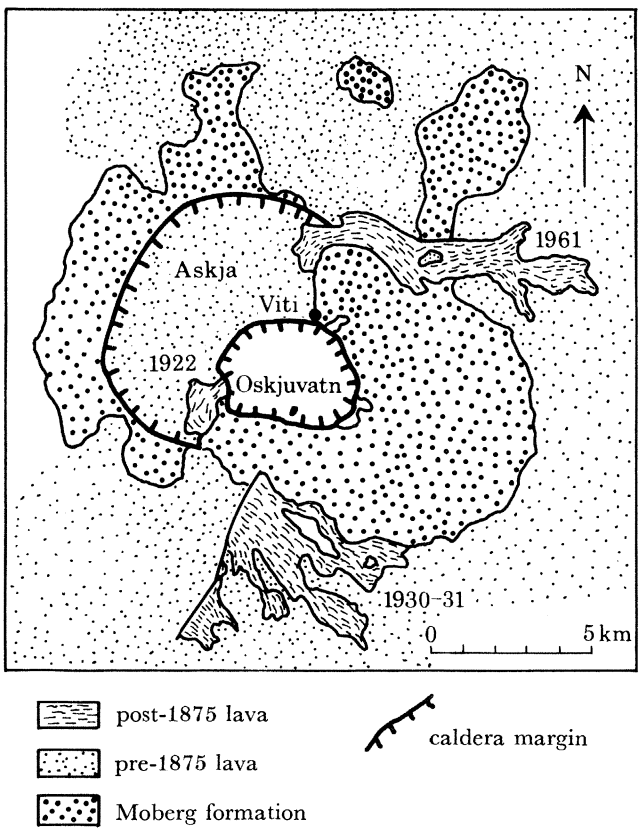

FIGURE 2. Geological map of Askja volcano modified after Sigvaldason (1964).

CHRONOLOGY

The 1874–75 rifting episode was preceded by severe earthquakes in the northern part of the eastern rift zone in April 1872 (Tryggvason 1973). One reached magnitude 6–7 and this activity was probably associated with major movements on the Tjornes fracture zone (figure 1). In February 1874 intense steam emission was noted at Askja. In the autumn of 1874 new fissures appeared in the Sveinagja area, 50–70 km north of Askja (figure 4), associated with increased seismic activity. By October 1874 the fissures had widened and were 'too wide to jump across' (Gudmundsson 1973). The formation of the graben in the Sveinagja fissure swarm preceded the basalt fissure eruption by several months. One week before Christmas, there was increased seismic activity in the northern rift zone and unconfirmed reports of volcanic activity in the northern Vatnajokull area. Earthquakes increased in number and intensity between Christmas and the New Year, becoming continuous, and were felt over all of northeast Iceland.

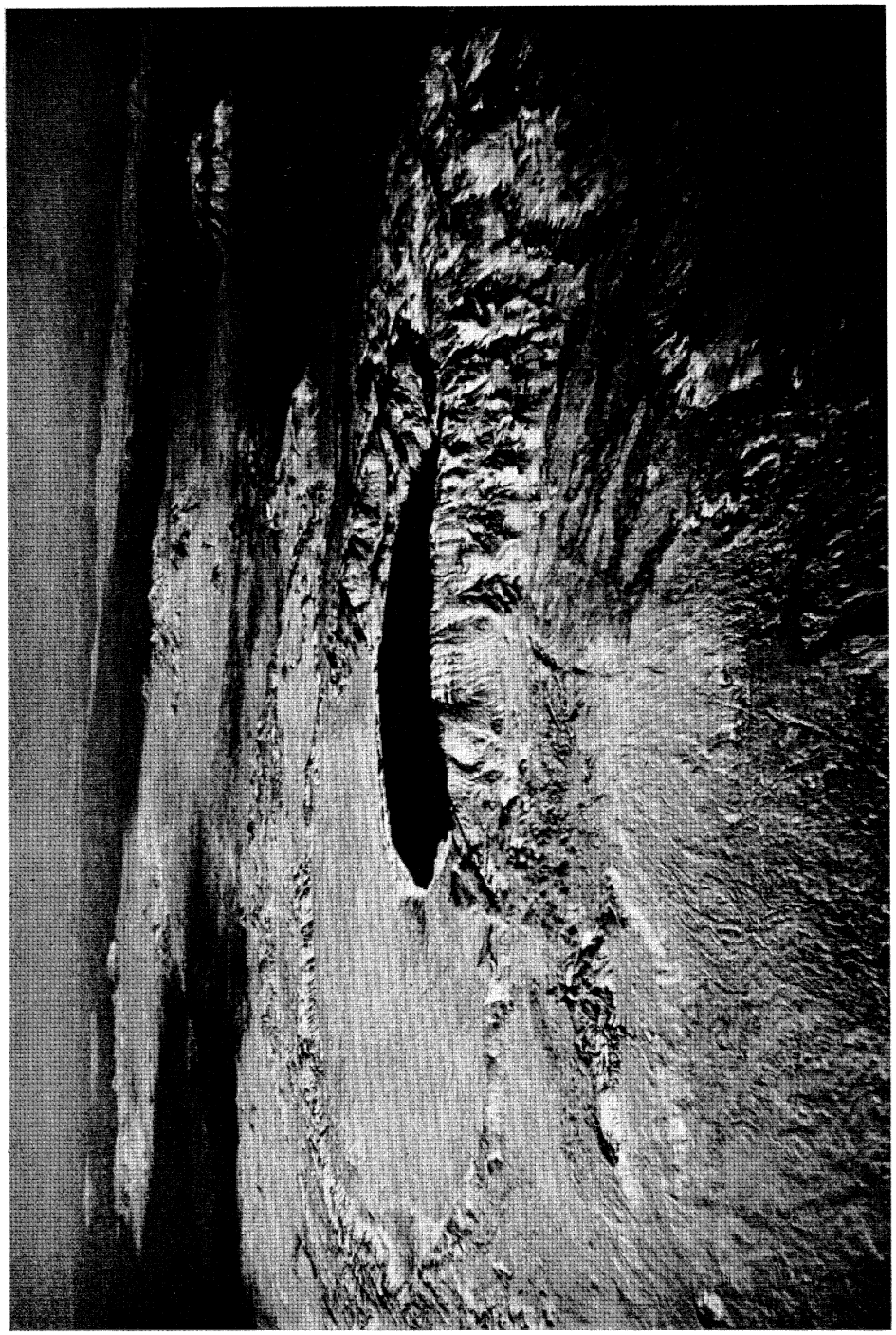

FIGURE 3. Oblique aerial photograph of the Askja central volcano looking to the north in winter. The large prehistoric caldera and 1875 caldera are clearly delineated. The rugged mountains to the east of Oskjuvatn are composed of palagonite tuffs, pillow lavas and pillow breccias (the Moberg formation). The table mountain, Herdubreid, is observed in the upper right corner. (Photography by O. Sigurdsson.)

(*Facing p.* 244)

PHILOSOPHICAL TRANSACTIONS OF THE ROYAL SOCIETY A MATHEMATICAL, PHYSICAL & ENGINEERING SCIENCES

FIGURE 6. Layers C and D are shown on the northwest rim of Oskjuvatn. The subdivision of layer C into two units is readily apparent here. The base surge climbing megaripple structures are observed in layer C_2. The zones of darkened pumices in layer D pass laterally into patches of welded tuff.

PHILOSOPHICAL TRANSACTIONS OF THE ROYAL SOCIETY A MATHEMATICAL, PHYSICAL & ENGINEERING SCIENCES

FIGURE 7. Layer C_2 on the eastern rim of Oskjuvatn showing well developed bedding, disconformities due to erosion by base surges and by melt-waters from snow. Contemporaneous faults are common in layer C.

FIGURE 8. Layers D and C 10 km east of Oskjuvatn at Drekagil. Layer C is thin here as the location is on the edge of the deposit off the dispersal axis. Layer D shows pronounced reverse grading.

PHILOSOPHICAL TRANSACTIONS OF THE ROYAL SOCIETY A MATHEMATICAL, PHYSICAL & ENGINEERING SCIENCES

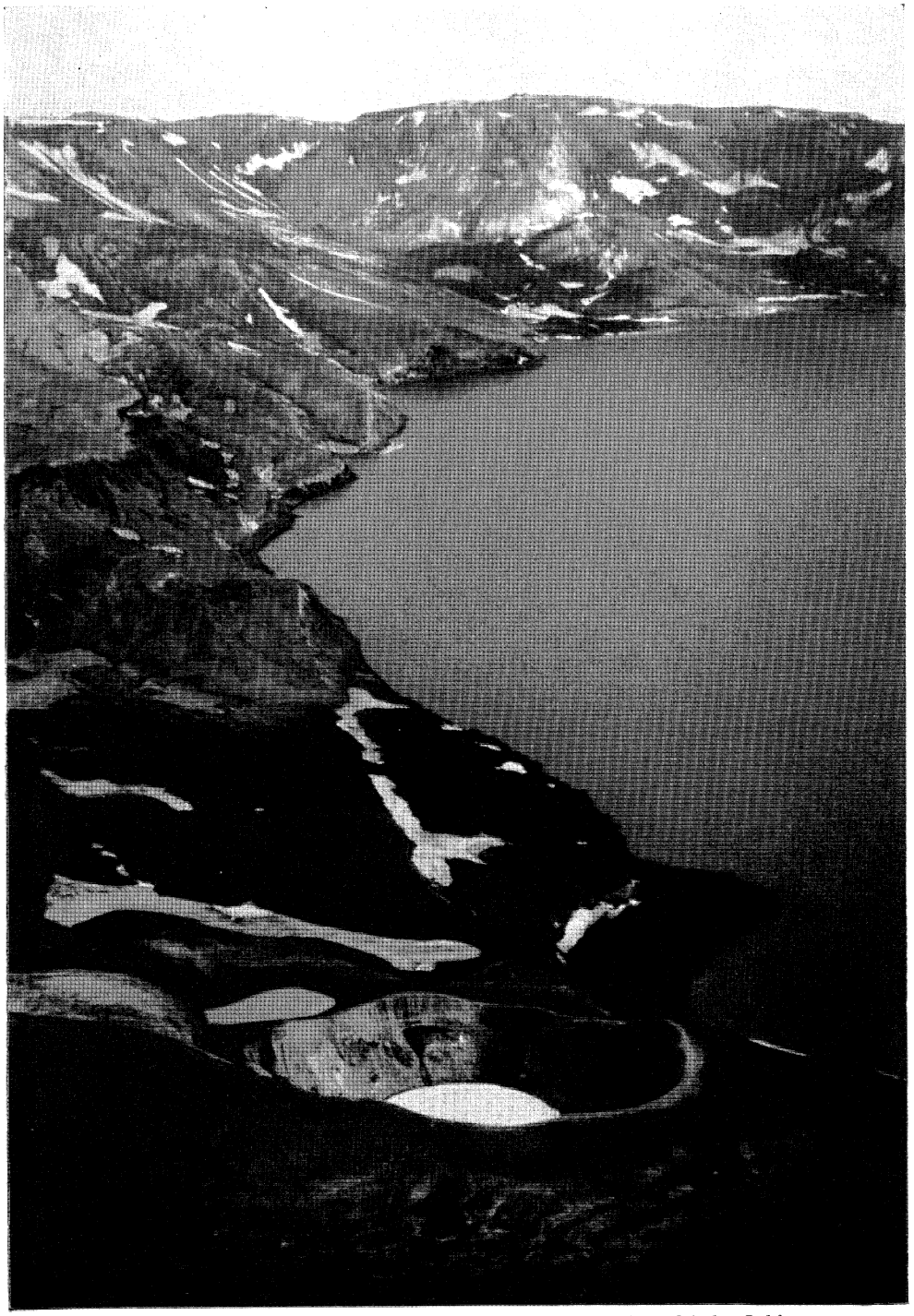

FIGURE 9. The Viti explosion crater and the northeastern edge of Lake Oskjuvatn. The 1924 aa lava flow is seen beyond Viti. (Photography by R. Greely.)

PHILOSOPHICAL TRANSACTIONS OF THE ROYAL SOCIETY A MATHEMATICAL, PHYSICAL & ENGINEERING SCIENCES

An eruption column was seen rising from the Askja region on 1 and 2 January 1875. Earthquake intensity and frequency was a maximum in the Myvatn region and continued until 8 January. Shortly before daybreak on 3 January, a column of fire was first observed above Askja. Seismic activity was intermittent for the next $2\frac{1}{2}$ months. A second eruption column was reported south of Askja. Minor ash-fall of dark ash and palagonitic dust was reported in Holsfjoll and Kelduhverfi, after the activity on 3 January. By 8 February earthquake activity had greatly subsided.

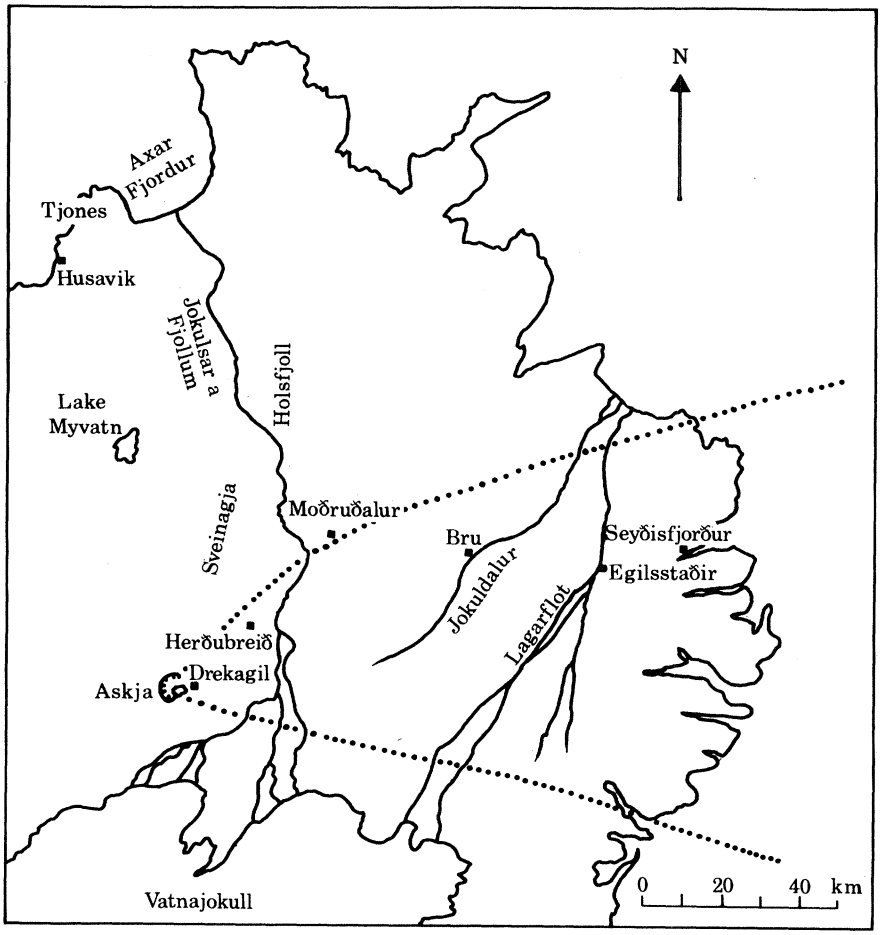

FIGURE 4. Map showing locations of places mentioned in text. Dotted lines show extent of 1875 ejecta.

On 16 February four farmers from Myvatn reached Askja. They found an active vent in the southeast corner of the Askja caldera, although it is unclear if the activity was phreatic or magmatic. A depression had formed some 200 m west of the crater with an area of 35 000 m^2; subsidence reached 10 m in the northeast, representing 350 000 m^3 of subsidence. A small lake had formed in the northwestern part. In the southern part of the depression a second crater was active, surrounded by a small lava flow, and a third, smaller crater was found to the west of this one. Continuous earth tremors occurred during their stay in Askja. These observations suggest that before 17 February 1875 there was only minor explosive activity. Subsidence perhaps represented the beginning of caldera formation.

On 18 February, the Sveinagja basaltic fissure eruption broke out, 70 km north of Askja,

along a 2–5 km long fissure. By 25 February, activity had ceased, but approximately 10^6 m^3 of basalt lava had been erupted. Activity was renewed on 10 March, 1.5 km further north on the Sveinagja fissure. There was active subsidence of the Sveinagja graben surrounding the active fissure, with subsidence of 60 cm observed on one day. On 23 March, activity was particularly vigorous on the northern part of the fissure where up to 40 fire fountains were observed. Activity then ceased temporarily in the Sveinagja fissure.

On 28 March, activity shifted to Askja, on the trend of the Sveinagja fissure. At 21h 00 on Easter Day, 28 March, a black eruption column rose above Askja and was observed clearly from Jokuldalur in the east; this marked the opening phase of the explosive eruption. Our knowledge of the sequence of events is based on observations made by farmers in inlying districts in eastern Iceland:

28 *March*

21 h 00 Black eruption cloud observed over Askja.

29 *March*

03 h 30 Minor ash-fall for one hour in districts 50 km east of Askja, accompanied by thunder and lightning. The ash was pale-grey, fine-grained and sticky. Ash-fall ceased for one hour.

06 h 30 Main pumice-fall starts over wide regions of eastern Iceland. The pumice-fall was so dense that total darkness resulted.

12 h 00 Pumice-fall stops in built-up regions of eastern Iceland.

Minor explosive activity was reported at Askja until the end of April at 5- to 7-day intervals, though no ash-fall was reported. On 4 April the Sveinagja fissure erupted again, continuing intermittently until 11 April. Minor activity was reported on 1 July and 13 July but the Sveinagja fissure remained quiet until 15 August when earth tremors were widely felt in the region, and activity was resumed with up to 20 fire fountains in the south part of the fissure. The last activity was reported on 20 October in the southernmost craters.

A major consequence of the 1874–5 volcanic–tectonic activity was the formation of the Oskjuvatn caldera (figures 2 and 3). W. L. Watts's observations in July 1875 described the caldera as being 3–4 km^2 in area and about 120–150 m deep. G. Caroc in 1876 surveyed the area and found that it covered 7 km^2 and had a depth of 232 m. Other parties (Thorarinsson 1963) record increasing areal coverage and a gradual filling of the depression with water. Today the caldera covers 11 km^2, and the northern rim of the caldera stands about 50 m above the lake level. The maximum recorded water depth is 217 m.

1875 Pyroclastic deposits

Stratigraphy

Figure 5 is a schematic section through the 1875 Askja products. We have divided the layers into those produced by minor precursory activity (notably on 3 January) and those produced during the 8½ hour paroxysmal eruption of 28–29 March. There is inevitably some uncertainty and ambiguity in relating historical observations and stratigraphic data. The section represents measurements taken on the northern and eastern rims of Oskjuvatn and is composite, as there is no one locality where every layer is found.

The lowermost rhyolitic lava flow was recognized as one of the eruption products by Sigvaldason (1968); it is exposed on the lake shore near Viti crater and 1 km to the southeast. The internal structure of the Viti lava outcrop is suggestive of an agglutinate formed by the rapid accumulation of spatter. The lava probably formed *before* 3 January 1875.

Layers A_1–A_3 are well preserved near Viti crater. A_1 is an orange ash layer composed predominantly of a mixture of fine to medium sand-sized vesicular obsidian fragments coated with white to red coloured sublimates and iron oxides. This layer is thought to represent the

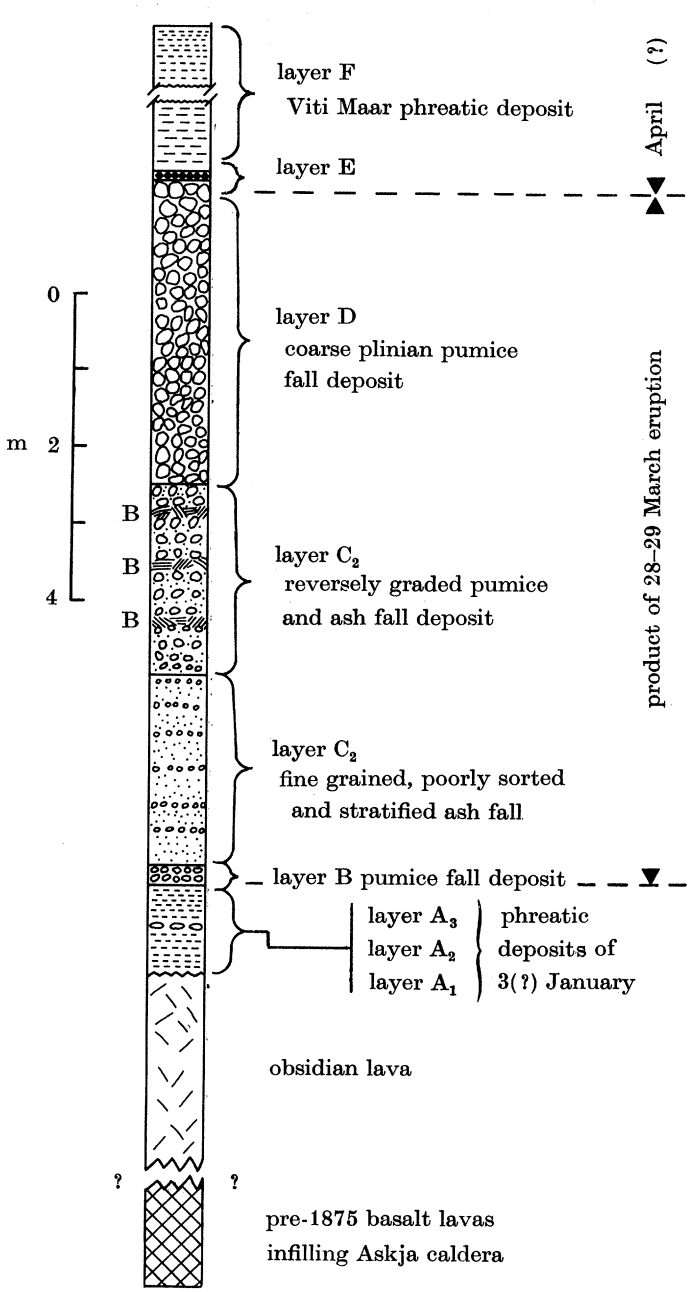

FIGURE 5. Schematic section of the products of the 1874–1875 period of activity of Askja. The thicknesses are the maximum observed on the northeastern rim of Oskjuvatn. B, on the right of the section, shows base surge horizons in layer C_2.

'palagonite ash' which fell in Holsfjoll and Kelduhverfi. Layer A_2 is a discontinuous band of rhyolitic scoria fragments. Layer A_3 is a very fine-grained pale gray layer similar in constituents to layer A_1, but finer grained and paler.

Layers B to E represent the products of the 28–29 March event. There is some uncertainty as to the stratigraphic position of layer B as there is no locality where it rests on layers A_1–A_3. Nevertheless, layer B is of plinian type and has an easterly dispersal like layers C–E, indicating that it represents the final products of the paroxysmal eruption. Layer B is a coarse, well-sorted, pumice-fall layer composed of white rhyolitic pumice and grey basaltic andesite pumice clasts.

Layers C_1 and C_2 can only be readily discriminated within the Askja caldera, and the transition between the two layers is always diffuse (figure 6, plate 2). Layer C_1 is everywhere extremely fine grained, composed of white, highly stratified ash (85% of less than 1 mm in diameter at Viti crater). There are, however, occasional larger, low-density pumice clasts present near the caldera. Well sorted lithic-rich horizons containing denser, grey pumice are locally present in layer C_1 around Oskjuvatn, but are not found away from the caldera margins. Layer C_2 is coarser grained (figure 6) with 50–65% of ejecta less than 1 mm in diameter at Viti crater. It is likewise poorly sorted and is highly stratified (figure 7, plate 3) owing to rapid fluctuations in grain size from one layer to another. Layer C_2 also has conspicuous base surge structures such as climbing megaripples with wave heights up to 1.5 m and wavelengths up to 6 m (figure 6), decreasing rapidly away from the caldera rim, as observed in other base surge deposits (Moore 1967; Crowe & Fisher 1973; Schmincke *et al.* 1973).

Beyond 5 km east of the Oskjuvatn rim the two layers C_1 and C_2 are no longer distinguishable, but are represented by a fine ash-fall layer which can be traced over 90 km from Askja (figure 8, plate 3). Fine sticky ash fell for an hour from 03 h 30 on 29 March, 50 km east of Askja, and we correlate this with the formation of layers C_1 and C_2.

Layer D represents the products of the main $6\frac{1}{2}$ h plinian phase. On the rim of Oskjuvatn it is a very coarse-grained, unstratified pumice-fall deposit (figure 6): only 10% of the ejecta in layer D is finer than 3.2 cm in diameter on the rim of Oskjuvatn. It is spread over 7500 km^2 of eastern Iceland (figure 4). Close to the source, layer D shows only slight reverse size grading. However, from 20 km to 80 km from the source, the deposit shows marked reverse grading (figure 8). Beyond 80 km the layer is thin and not obviously graded.

Above layer D there is near-source surface layer (layer E in figure 5) of lithic fragments composed of non-vesicular rhyolitic obsidian, partially fused trondjheimite xenoliths (often vesicular breadcrust bombs), and basalt fragments, in the proportions given in table 5. The same lithic assemblage occurs in every low abundance in the plinian layer D. The trondjheimite xenoliths are also found occasionally within large pumice bombs in layer D, suggesting that at least some were immersed in the rhyolitic magma body. Layer E may be due to vulcanian-style explosions in April which disrupted an obsidian lava dome or plug. Alternatively lithics may have been concentrated as a surface layer by winds since 1875.

The Viti crater, situated on the northeast edge of the Oskjuvatn caldera (figures 2, 3 and 9, plate 4) was previously regarded as the source vent for the main pumice eruption, but this can be disproved by data on thickness and grain size (see below). The deposits from Viti consist of highly stratified, fine grained, brown tuffs which form a distinct 12 m high rim around Viti (figure 9). These products decrease to 1 m thick 50 m from the crater rim and are not preserved beyond 150 m. They are typical of phreatic deposits, being composed largely of non-juvenile lithic fragments, derived during excavation of the crater, set in a muddy, clay-rich matrix.

There are also some obsidian fragments, suggesting a juvenile component in the explosions. Much of the material fell as mud droplets during phreatic explosions, forming a porous tuff which is composed of round pellets of mud.

An important facies of the Askja pyroclastics is zones of densely welded tuff. Some discontinuous lenses are developed along the northern rim of Oskjuvatn in layer D (figure 7), but the main outcrop covers 1.6 km² on the southwestern edge of Oskjuvatn, where densely welded rock is found up to 6 m thick. The welded zone can be correlated with the upper parts of layer C_2, which becomes darkened along the western rim and then passes laterally into a welded tuff. The welded tuff mantles the surrounding palagonite tuff ridges, as well as forming a sheet over the old prehistoric caldera floor. The welded facies are described in detail by Sparks & Wright (1979).

TABLE 1. CHEMICAL ANALYSES OF ASKJA EJECTA

	1	2	3	4	5	6	7	8	9	10	11
SiO_2	73.72	73.06	71.55	74.89	51.16	52.21	59.00	72.37	72.95	75.06	63.54
Al_2O_3	12.81	12.84	13.19	12.89	14.17	12.80	14.53	12.66	12.80	12.50	13.96
TiO_2	0.80	0.86	1.00	0.57	1.85	2.23	1.78	0.92	0.50	0.45	1.19
FeO	3.34	3.46	4.78	2.60	12.92	14.31	10.05	3.85	4.21	1.88	7.09
MgO	0.60	0.70	0.88	0.36	6.45	4.84	2.57	0.69	0.50	0.27	2.70
CaO	2.31	2.57	3.43	2.55	10.08	8.94	6.14	2.52	1.93	0.64	5.85
Na_2O	3.65	3.67	3.25	3.95	2.05	3.00	3.38	3.85	4.17	3.31	3.38
K_2O	2.40	2.37	2.09	2.55	0.20	0.64	1.34	2.31	2.09	3.52	1.51
P_2O_5	0.14	0.12	0.12	0.09	0.21	0.21	0.67	0.03	0.12	0.20	0.16
MnO	0.08	0.09	0.10	0.05	0.27	0.14	0.21	0.04	0.10	0.10	0.16
H_2O	—	—	—	—	—	—	0.24	—	0.65	—	0.32
total	99.85	99.74	100.39	100.50	99.36	99.28	99.91	99.24	100.02	98.93	99.86

1. Clear rhyolitic glass (average of 27 analyses).
2. Brown rhyolitic glass (average of 23 analyses).
3. Example of iron-rich rhyolitic glass (average of 3 analyses).
4. Example of iron-poor rhyolitic glass (average of 3 analyses).
5. Basaltic glass from obsidian bomb ejected in late stages of layer D phase (average of 9 analyses).
6. Basaltic andesite glass from grey pumice in layer B (average of 3 analyses).
7. Bulk composition of crystal-rich grey andesite pumice inclusions in white pumice of layer D (average of 4 analyses).
8. Interstitial glass of crystal-rich grey andesite pumice inclusions in white pumice of layer D (average of 3 analyses).
9. Whole rock analysis of partially fused granodiorite xenolith (sample As 15).
10. Glass analysis of partially fused zenolith (sample As 15: average of 3 analyses).
11. Whole rock analysis of physically mixed grey pumices from 4 localities of layer D (average of 4 analyses).

Varieties of ejecta and their composition

Layers B–D are composed of several lithological components. Over 92% is white rhyolitic pumice which is almost devoid of any phenocrysts. Close to the source, large pumice clasts in layer D are coloured cream to rose-pink. The white pumice consists of clear rhyolitic glass (table 1, analysis 1). The glasses show a considerable degree of heterogeneity. Individual analyses range from varieties rich in FeO, MgO, TiO_2 and CaO and relatively low in SiO_2 content (table 1, analysis 3) to glasses which have lower FeO, TiO_2 and CaO contents and high SiO_2 contents (table 1, analysis 4). Phenocrysts (1–1.5%) of plagioclase (An_{44}–An_{60}), clinopyroxene and titanomagnetite occur together with occasional orthopyroxene and ilmenite.

The second most abundant ejecta type which can be distinguished in the field is pale to dark-grey pumice. Subsequent petrographic study has enabled us to recognize *three different kinds* of grey pumice.

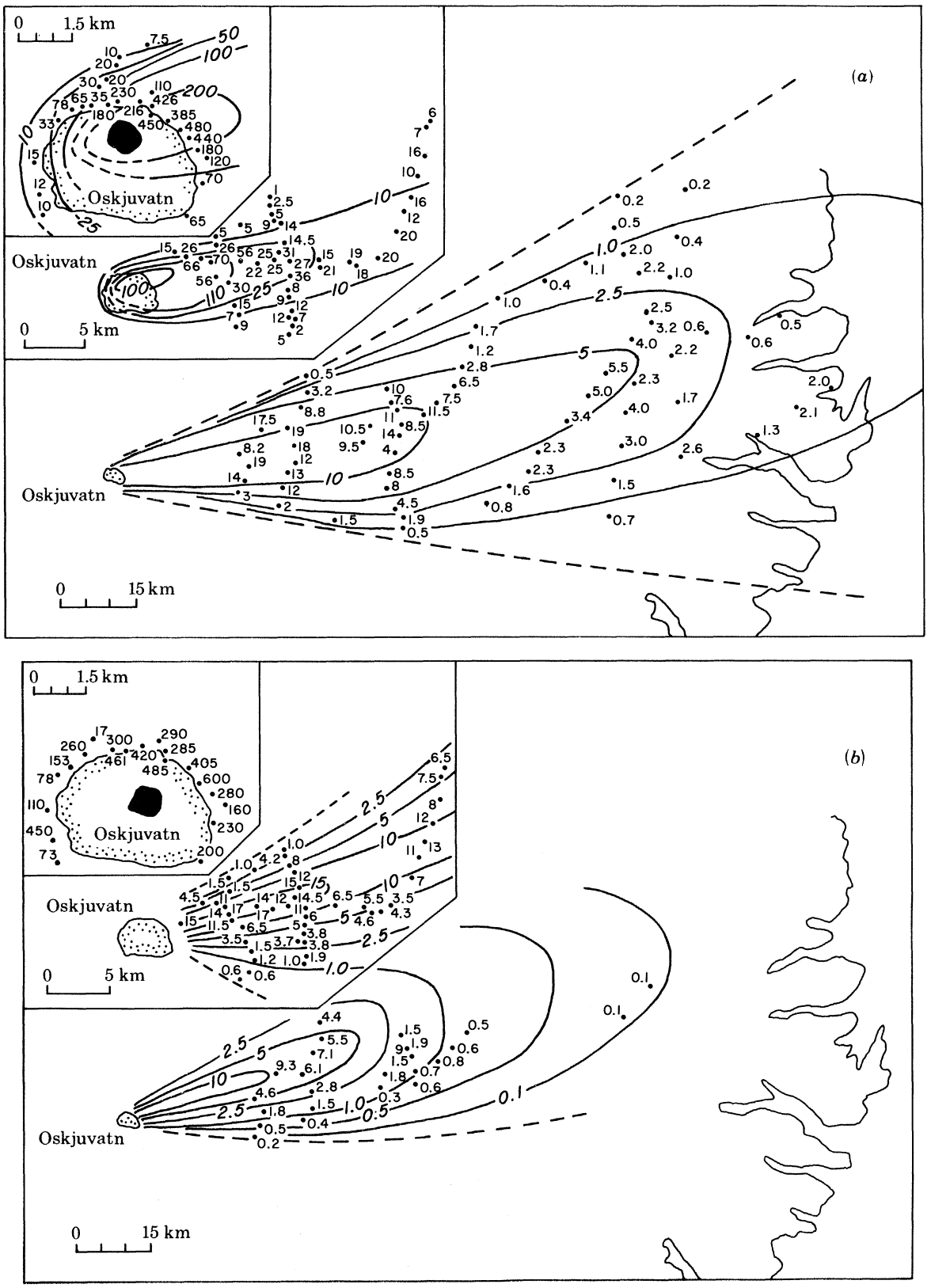

FIGURE 10 (*a*, *b*). Isopach maps of (*a*) layer D, (*b*) layer C. Source shown by darkened area; thickness in centimetres.

The first is grey pumice, because of high emplacement temperature. Near Viti crater the plinian layer D contains an upper and lower zone of dark, steel-grey pumice (figure 6). Traced along the northern rim of Oskjuvatn these dark-grey pumice zones merge into lenticular areas of welded tuff, whereas to the east the coloured zones rapidly die out.

The second and most important kind constitutes approximately 5% by mass of layers B–D. These are pale to dark-grey pumice clasts composed of exceedingly intimate mixtures of rhyolitic and basaltic glass. The grey pumice occurs largely as discrete fragments recognizable to over 100 km from source. Few exceed 2 cm in diameter, but pumice clasts are occasionally found containing bands of the grey pumice mixed within white pumice. The grey pumice is composed of brown rhyolitic glass, and inclusions and streaks of dark brown basaltic glass.

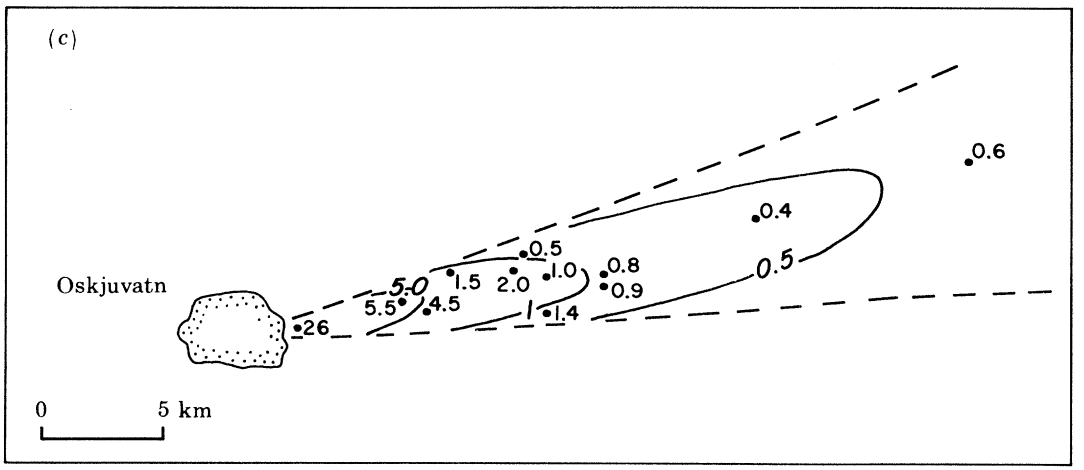

FIGURE 10(c). Isopach for layer B.

Table 1 (analysis 2) shows the average composition of the brown rhyolitic glass. The chemistry of the basaltic glasses is variable, and table 1 (analysis 5) gives average analyses of glass in an obsidian block ejected in the late stages of the layer-D phase. Phenocrysts of plagioclase (An_{73}–An_{90}) and pyroxene ($Wo_{37}En_{40}Fs_{23}$ to $Wo_{39}En_{43}Fs_{20}$) are abundant, and titanomagnetite and olivines are occasionally observed. In layer B the glass compositions of the basic component in the grey pumice clasts are basaltic andesite (table 1, analysis 6).

The third type is found as occasional pale-grey pumiceous inclusions (about 0.75% by mass) of crystal-rich andesite which occur as irregular blobs and occasional streaks in the white pumice. These inclusions are denser than the rhyolitic pumice and have spherical microvesicles. They are rich in plagioclase (An_{44}–An_{51}) and pyroxene microphenocrysts (Wo_{35} En_{42} Fs_{23}–Wo_{40} En_{40} Fs_{20}), with abundant titanomagnetite and ilmenite, and some apatite laths, set in a vesicular rhyolitic glass. Their whole rock compositions are andesitic (table 1, analysis 7). whereas their rhyolitic glass matrix (table 1, analysis 8) is indistinguishable from the surrounding rhyolitic glass. The andesite inclusions range from a few tens of micrometres to 1 cm in diameter,

Lithic clasts make up about 2% by mass of layers B–D and all of layer E. Rhyolitic obsidian fragments are composed of the same components as the vesicular ejecta: clear and brown rhyolitic glasses, basaltic glasses and andesitic inclusions can be sometimes observed intimately associated in a single thin section of obsidian. The partially fused and vesicular trondjheimite xenoliths typically contain 50% glass (table 1, analysis 10), and their whole-rock compositions

PHILOSOPHICAL TRANSACTIONS OF THE ROYAL SOCIETY A MATHEMATICAL, PHYSICAL & ENGINEERING SCIENCES

are similar to the rhyolite (table 1, analysis 9). Other lithics include crystalline and altered basalt fragments.

Thickness variations

Figure 10 shows isopach maps of the principal layers formed in the 28–29 March eruption. All the layers show easterly dispersal. The isopach map for layer D (figure 10*a*) is similar to that produced by Thorarinsson (1944) based on thicknesses measured shortly after the eruption except for those beyond 100 km on the east coast of Iceland. The discrepancy is caused by the difference in the thickness of freshly fallen, fine-grained ash compared to compacted ash.

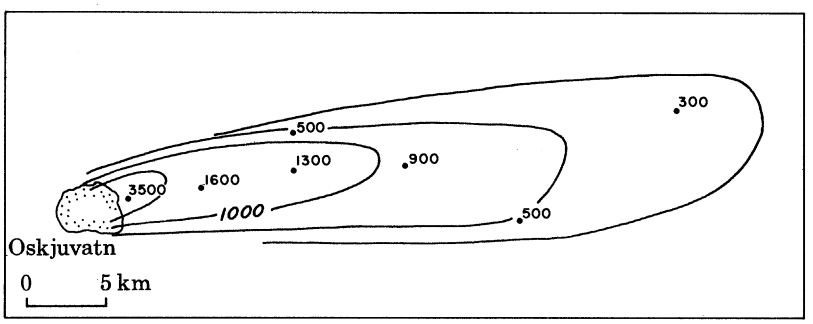

FIGURE 11. Isopleth map of accumulation in grams per square metre for layer E.

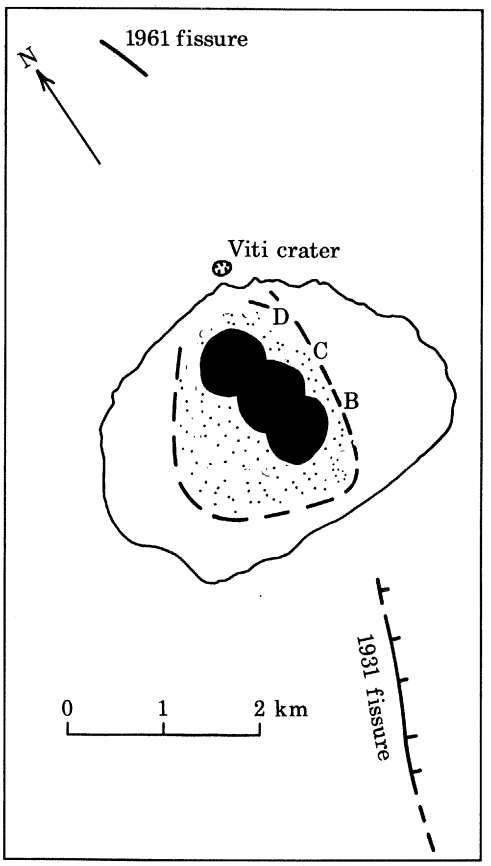

FIGURE 12. The postulated positions of the vent of each of the phases of the 1875 Askja eruption within Oskjuvatn.

Several processes have modified thicknesses since 1875. Between Askja and Jokulsa à Fjollum, æolian dunes have formed in layer D, and original thicknesses are often difficult to establish. The distal ash has been incorporated in the loess soil and has often been disrupted by roots. The distal ash is sometimes observed to thicken in depressions; several measurements were taken and the results averaged. Despite these uncertainties, our measurements are generally accurate to within 10 % of the compacted ash thickness. Layers A, B and C are protected by layer D, and so generally the problems of post-depositional redistribution are less serious. Layer E, however, is too thin to provide meaningful isopachs. The lithic clasts from layer E were collected from a 1 m² area and weighed (figure 11).

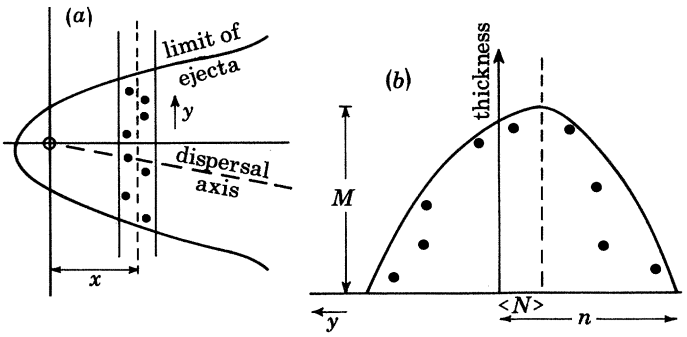

FIGURE 13. Method of determining volume of pyroclastic fall deposits defining terms discussed in text: (*a*) plan view of ejecta dispersal, showing strips; (*b*) cross section of strip.

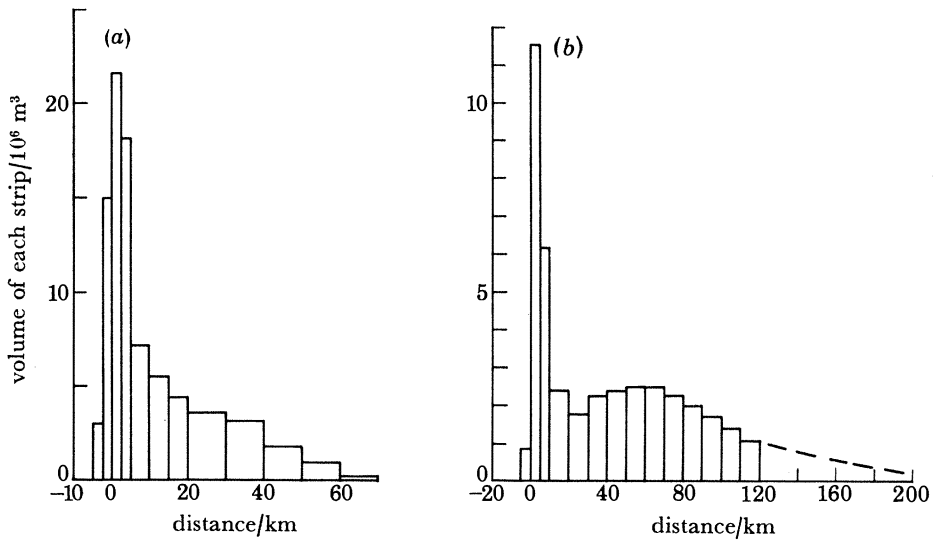

FIGURE 14. Volume of tephra in strips 2.5, 5 and 10 km in width normal to the dispersal axis: (*a*) layer C; (*b*) layer D.

TABLE 2. ESTIMATES OF TEPHRA VOLUMES OF THE 1875 EJECTA IN UNITS OF CUBIC METRES

layer	observed volume	Missing volume	total volume	error
B	2.67×10^6	5.6×10^5	3.23×10^6	18 %
C	1.57×10^8	8.5×10^6	1.66×10^8	4 %
D	5.67×10^8	4.6×10^7	6.13×10^8	8 %
E	5.00×10^8	—	5.00×10^5	—
total	7.27×10^8	5.51×10^7	7.82×10^8	8 %

Walker (1973) has suggested a method of comparing the relative dispersal areas of pyroclastic fall deposits. He proposes a parameter D which is the area enclosed by the 0.01 T_{max} isopach contour, where T_{max} is defined as the maximum thickness at source, estimated by extrapolation of thickness–distance data. The D-values are as follows: layer B, 100 km²; layer C, 400 km²; and layer D, 2000 km², demonstrating an increase in dispersal as the eruption progressed. This is matched by an increase in maximum grain size of each layer (see below), suggesting that the height of the eruption cloud increased with time.

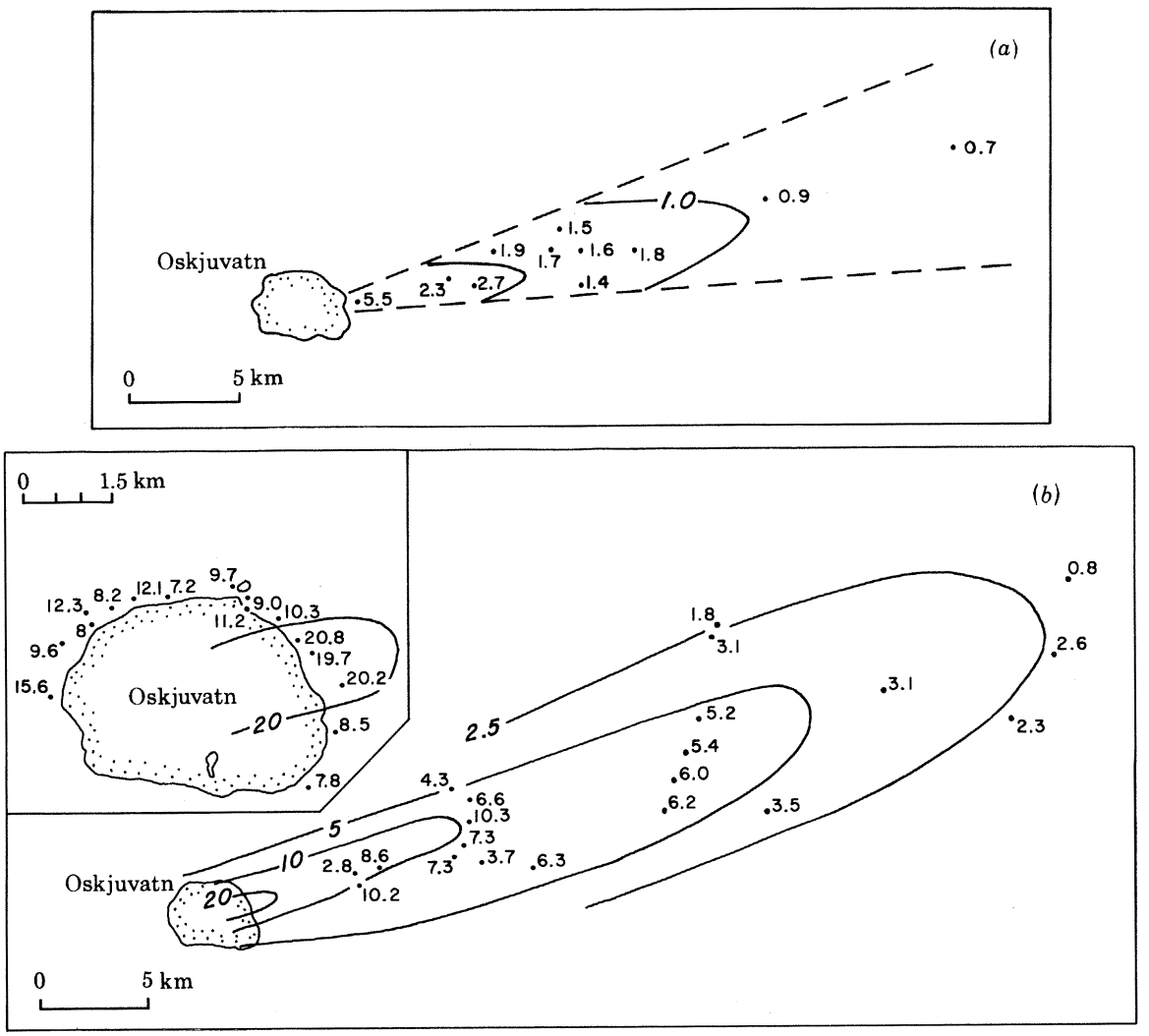

FIGURE 15 (*a*, *b*). Maximum grain size isopleth maps showing the average diameter in centimetres of the five largest pumice clasts at each location: (*a*) layer B; (*b*) layer C.

Layer B has a well-constrained dispersal envelope (figure 10*c*) which indicates a source vent in the south-central part of Oskjuvatn. In layer C (figure, 10*b*) the isopach contours indicate a vent north of that for layer B, in the central part of Oskjuvatn. The isopach maps for layers D and E (figures 10*a* and 11) indicate a vent in the northern half of Oskjuvatn. The last event of the eruption formed Viti crater which is still further north. These trends are confirmed by maximum grain-size data. The data are most easily explained by activity along a north–south

trending line of vents, 1.5 km long, through the centre of Oskjuvatn with the locus of activity shifting northwards as the eruption progressed (figure 12). The broad north–south trending zone of activity may be a line of weakness which controlled the position of the 1924 and 1929 eruptions (figure 12), or the ring fracture of the old Askja caldera.

Volumes were estimated by the following method. Each isopach map was divided into a number of north–south strips, ranging in width from 1 to 10 km. All the sample points in a

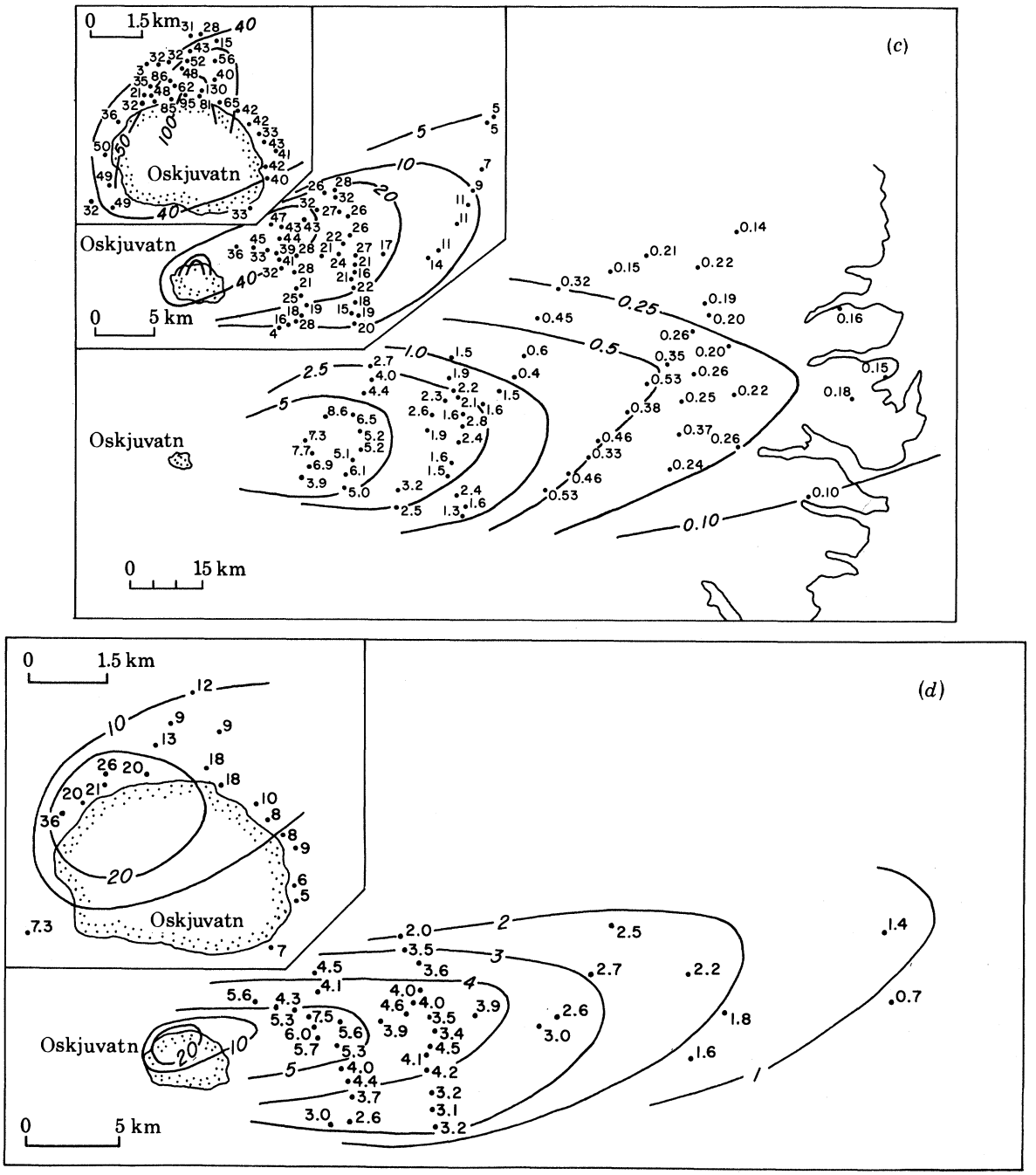

FIGURE 15 (*c*, *d*). Maximum grain size isopleth map for (*c*) layer D and (*d*) layer E.

PHILOSOPHICAL TRANSACTIONS OF THE ROYAL SOCIETY A MATHEMATICAL, PHYSICAL & ENGINEERING SCIENCES

strip were assumed to be the same distance from an arbitrary north–south line which passes through the vent location: thus their northerly coordinates were kept fixed but their easterly coordinates were adjusted to the centre of the strip. The thickness of each sample point was then plotted on a graph of thickness against distance north of the dispersal axis (see figure 13*a* for illustration of the method). The parabolic curve that enclosed all the data points was determined, to generate the parameters m, n and N which are graphically defined in figure 13*b*. The volume in each strip was then $1.333mnA$, where A is the width of each strip. The volume for each strip was then plotted as a function of distance downwind. Such plots for layer C and D are shown in figure 14. The volume–distance data were then extrapolated downwind. Table 2 shows the observed volume and the missing volume estimated from extrapolation of the data.

We have computed a total volume of 0.61 km³ for layer D both on land and sea which yields a total tephra volume of 0.8 km³ for the eruption. This figure is similar to the land-based estimate of Thorarinsson (1944, 1963, 1971). By using the data in figure 14, the amount lost to sea is estimated as only 7.5% of the total. There are many uncertainties in the extrapolation. For example, the volume–distance relation of a pyroclastic-fall deposit partly depends on the total grain size population of the ejecta, and if the D-phase of the eruption had produced a large quantity of fine ash, much may have blown out to sea. Very fine ash of a few tens of micrometres in diameter reached Scandinavia (Mohn 1898; Persson 1967). We demonstrate later that layer D has an additional population of fines superimposed on a broad population of grains, and much of this additional population of fines was lost to sea.

The measured density of layer D varies from 0.45 g/cm³, 10 km from the source, to over 0.7 g/cm³ at Bru. Taking a mean value of 0.6 g/cm³ and an original magma density of 2.3 g/cm³, we estimate 0.21 km³ of dense rhyolitic magma for layers A–E. The bathymetric map of Oskjuvatn by S. Rist (Thorarinsson 1963) indicates that the total volume of missing material can be computed as 2.0 km³. There is a discrepancy of 1.8 km³ between the caldera volume and the volume of ejected magma.

A notable feature of layer D is a bimodality in the volume against distance relations (figure 14). This is interpreted as a reflexion of the unusual grain-size characteristics of the ejecta, which are polymodal with an overabundance of ash-sized particles apparently accumulated in the distal parts of the layer beyond 60 km.

Granulometric studies

Maximum grain size

Figure 15 shows data on maximum grain size isopleth maps of the main layers. Each fragment was treated approximately as an ellipsoid; the minor, intermediate and major axial dimensions were recorded, and the equivalent spherical diameter calculated. At each site the equivalent diameter of the five largest clasts were averaged to generate the data in figure 15. The largest single bomb was measured 1 km west of Viti and 100 m from Oskjuvatn rim: $7.6 \times 6.2 \times 1.4$ m with a density of 0.9 g/cm³, a total mass of 29 tonne.

The data show that the whole sequence is reverse graded; that is, at any location the maximum grain diameter increases with stratigraphic height. This complements the increasing dispersal of successive layers and indicates progressive increase in intensity of the eruption with time.

In layer D (figure 15) the 100 cm and 50 cm isopleths have northerly trending dispersal axes and the 40 cm isopleth axis trends northeast, whereas the smaller diameter isopleths are distributed to the east in a manner consistent with the prevailing wind direction. The northerly dispersal of large clasts is not reflected in the isopach map and (figure 10*a*) is considered the consequence of an angled vent. The lower, high-speed part of the column was angled to the north, at an angle sufficient to discharge large pumice bombs in a northerly direction. Pumice bombs larger than 50 cm in diameter behaved in a ballistic fashion, and their dispersal is controlled by the vent angle and not by wind direction. Pumice bombs between 50 and 20 cm in diameter are affected by both wind and vent angle, and have a dispersal axis oriented to the northeast. As the grain diameter decreases, the effect of wind becomes dominant, and the wind completely controls the easterly dispersal of the Askja ejecta of less than 20 cm diameter. Studies of bombs ejected during the 1973 Heimaey eruptions (Self *et al.* 1974) suggest a value of 40 cm for the bomb diameter above which the wind has little effect.

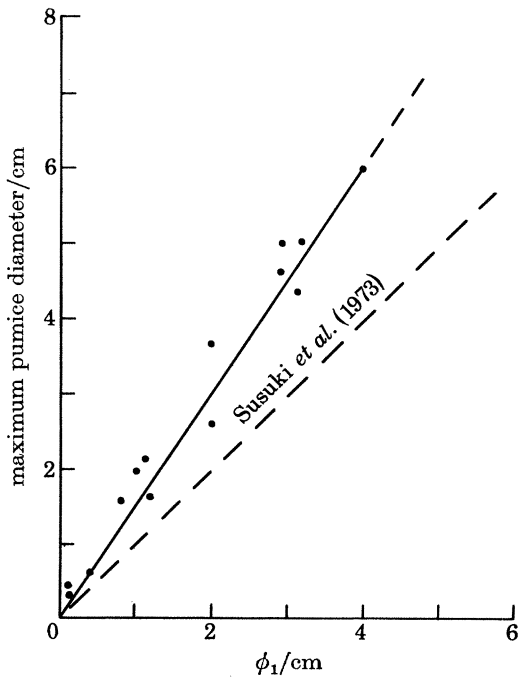

FIGURE 16. A plot is shown of maximum grain size (average of the five largest pumice clasts) against the coarsest one percentile from sieve analyses.

The observed maximum grain-size measurements are very close to the 'absolute' maximum grain size because of the almost complete preservation of near-source ejecta as a continuous sheet. In prehistoric plinian deposits, however, such measurements are generally made on vertical exposures, and the sample area is substantially reduced. Two localities on the rim of Oskjuvatn and one locality at Drekagil (figure 4) were chosen to examine the differences between vertical and surface measurements. The average equivalent diameter on the upper surface of the deposit was almost twice that of extracted pumices from the vertical exposures: 65, 28; 52, 21; and 41, 22 cm being the respective pairs of data. Measurements of maximum grain size in vertical sections close to the vent can substantially underestimate the true maximum size in prehistoric deposits. These data are commonly used to estimate gas-exit or muzzle

velocities (Fudali & Melson 1969; Wilson 1972, 1976), and thus the estimates of gas velocities derived in this manner are probably minimum values in older deposits.

There is a good correlation between average maximum grain size and the coarsest one percentile from samples sieved from the same locality (figure 16); the data lie on a line which indicates that the average diameter of the five largest fragments is 1.5 times larger than the coarsest one percentile. This compares with Suzuki *et al.* (1973) who show a 1:1 correlation of ϕ_1 and the average diameter of the ten largest fragments.

TABLE 3. GRAIN SIZE ANALYSES

	1	2	3	4	5	6	7	8	9	10	11	12
−9	10.0	—	—	—	—	—	—	—	—	—	—	2.7
−8	21.8	5.0	3.3	—	—	—	—	—	—	—	—	6.2
−7	20.9	29.0	5.4	—	—	—	—	—	—	—	—	6.1
−6	25.1	38.3	19.6	—	—	—	—	—	—	—	—	7.2
−5	11.0	21.0	34.5	23.8	14.0	4.2	2.2	—	—	—	—	7.1
−4	8.1	5.3	18.0	35.0	32.1	14.4	9.4	1.4	—	—	—	7.5
−3	1.9	0.7	11.0	20.0	23.9	24.6	26.9	7.9	—	—	—	7.9
−2	0.5	0.8*	5.3	10.6	15.8	26.8	23.3	33.7	1.1	—	—	7.8
−1	0.2	—	1.5	3.5	6.6	14.1	14.0	23.2	8.0	0.6	—	7.3
0	0.2	—	0.6	2.5	3.9	8.0	10.1	15.8	21.2	10.4	0.8	8.5
1	0.1	—	0.3	1.3	1.7	4.2	5.0	6.6	28.5	38.9	21.8	12.5
2	0.1	—	0.3*	1.0	0.8	1.6	2.3	3.4	12.3	28.2	38.1	8.4
3	0.1*	—	—	0.9	0.4	1.0	3.0	2.9	10.6	9.4	18.5	4.6
4	—	—	—	1.1	0.7	1.2	3.9*	5.2*	10.4	9.0	14.0	3.3
			—	—	—	—	—	—	7.9	3.6	6.8	3.0

1. Layer D; 1 km SE of Viti on eastern rim of Oskjuvatn.
2. Layer D; 1.2 km west of Viti on northern rim of Oskjuvatn.
3. Layer D; at mouth of Drekggil 7 km down dispersal axis.
4. Layer D; 13 km down dispersal axis.
5. Layer D; 18 km down dispersal axis.
6. Layer D; 28 km down dispersal axis.
7. Layer D; average of three analyses, 36 km down dispersal axis.
8. Layer D; 58 km down dispersal axis.
9. Layer D; 70 km down dispersal axis.
10. Layer D; 10 km down dispersal axis.
11. Layer D; 145 km down dispersal axis.
12. Layer D; total grain size distribution up to 150 km from source.

Grain size analyses

From the various layers 126 samples were collected for granulometric analysis. They were sieved with a set of sieves at 1 phi (ϕ) interval, where $\phi = -\log_2 r$, r being the diameter of the sieve mesh in millimetres. 32, 16 and 8 mm mesh sieves were taken into the field and these coarse fractions were sieved *in situ* to minimize breakage, and so that large representative samples could be treated for coarse grain analysis. Clasts greater than 32 mm were measured individually and the three ellipsoidal axes were recorded. Studies of pumice densities in the field (see below) allowed these data to be converted to mass percentage. Cumulative curves were drawn on probability paper from which the parameters median diameter Md_ϕ, the graphical standard deviation σ_ϕ and first-order skewness α_ϕ could be determined. Md_ϕ is defined as the ϕ-value where the cumulative curve crosses the 50 % line and $\sigma_\phi = \frac{1}{2}(\phi_{84} - \phi_{16})$. Table 3 shows selected analyses of the Askja layers. The skewness (α_ϕ) is defined by Inman (1952) as:

$$\alpha_\phi = \frac{\frac{1}{2}(\phi_{84} + \phi_{16}) - Md_\phi}{\sigma_\phi}.$$

The most difficult samples to sieve were the coarse-grained proximal parts of layer D. The pumice is often very brittle and breaks up during sampling. We excavated fresh material at three localities, and picked out and measured each pumice clast individually (table 3, analyses 1–3). In addition, traverses of 500 m length and 50 cm width were made over the upper surface of the deposit to document the number of pumice clasts greater than 25.6 cm in diameter. The median grain size of the three samples lies in the range 8 to 15 cm (-6 to -7.5ϕ) and, when compared with other plinian deposits at similar locations (Fisher 1964; Kittleman 1973), these are the coarsest pumice deposits yet documented. We do not believe that the Askja plinian layer is unusual, but attribute these differences to the more complete preservation of the deposit, and the field techniques used.

On the margins of the plinian layer the deposit thins from a continuous cover of pumice to isolated piles of pumice blocks. The areal density of these piles decreases to one pile per 50 m^2 at the northern edge of the dispersal area near the 1961 Askja basalt lava. These piles represent pumice blocks that have broken up on impact. All gradations can be found, from wholly preserved pumice bombs and bombs partially broken along joints, which could be reconstructed like a jigsaw, to piles of randomly oriented pumice fragments. The broken pumice clasts are angular and are the result of breaking along orthogonal joints which often parallel fibrous and tabular structures in the vesicles. The spacing of the joints and size of pumice blocks is regular, typically 2–8 cm. Pumices that did not break up on impact are by contrast ragged and irregular. The joints are interpreted as cooling cracks. The blocks were still hot on impact. The same impact breakage featured in Hekla pumice deposits shortly after the 1947 eruption (Thorarinsson 1954). Impact breakage in these proximal localities is evidently substantial. The median grain diameter of the airborne ejecta may be at least three and possibly as much as six times greater than the deposit.

These observations pertain to a problem in prehistoric plinian pumice deposits. Many workers (Walker & Croasdale 1971; Lirer *et al.* 1973; Self 1976) have observed that pumice and lithic clasts in plinian deposits are hydraulic equivalents except near source. Lithics are smaller than pumices because of their greater density. In many plinian deposits the maximum pumice–lithic diameter ratio becomes progressively smaller as the source is approached, and often becomes less than one near the source (Self 1976; Booth *et al.* 1978). The observations at Askja suggest that this relation is due to pumice breakage close to the vent. Lithics are generally much more coherent, and usually cold; so the amount of breakage is therefore small. Pumice break-up is only substantial for coarse grains. Thus pumice and lithics are hydraulic equivalents beneath a certain grain size: generally less than a few centimetres. Lithic grain-size data, if present, should be used in preference to pumice grain-size data in calculations on eruptions dynamics.

Grain size variations

Figure 17 is a plot of Md_ϕ against σ_ϕ for the Askja layers, showing the pyroclastic fall and flow deposit fields after Walker (1971). Layers D and B are uniformly well sorted (σ_ϕ varies from 0.6 to 1.8) which is typical of plinian air-fall deposits (Walker 1971, 1973). Layer C shows important contrasts in the lateral variations of Md_ϕ and σ_ϕ as compared with layers B and D. In layers B and D, Md_ϕ decreases rapidly with distance from the source (figure 18*a*). Layer C, however, shows little change of Md_ϕ away from the source (figure 18*b*). Layer D shows no relation between σ_ϕ and distance from source. Layer C, however, shows a clear decrease in σ_ϕ with distance from the source (figure 19).

Layer D is coarser than several other plinian fall deposits (figure 18*c*) in that the deposit has a larger value of Md_ϕ than other documented examples at any given distance from source (compare Fisher 1964; and Kittleman 1973). The shapes of the frequency curves downwind (figure 20*a*) are similar but are shifted to smaller grain-size fractions with distance from source; the slopes of the coarse and fine tails are parallel (distribution grading). Many plinian air-fall deposits show similar downwind sorting: for example, the Pompeii and Avellino deposits (Lirer *et al.* 1973), the 1563 and Fogo A deposits, São Miguel (Walker & Croasdale 1971), the Toluca pumice deposit (Bloomfield *et al.* 1977), the 1667 Tarumai pumice fall deposit (Susuki *et al.* 1973) and several sub-plinian deposits on Teceira, Azores (Self 1976). This style of downwind sorting is explained by a high, vigorous eruption column, and wind transport of the plume from which particles settle out according to size and density.

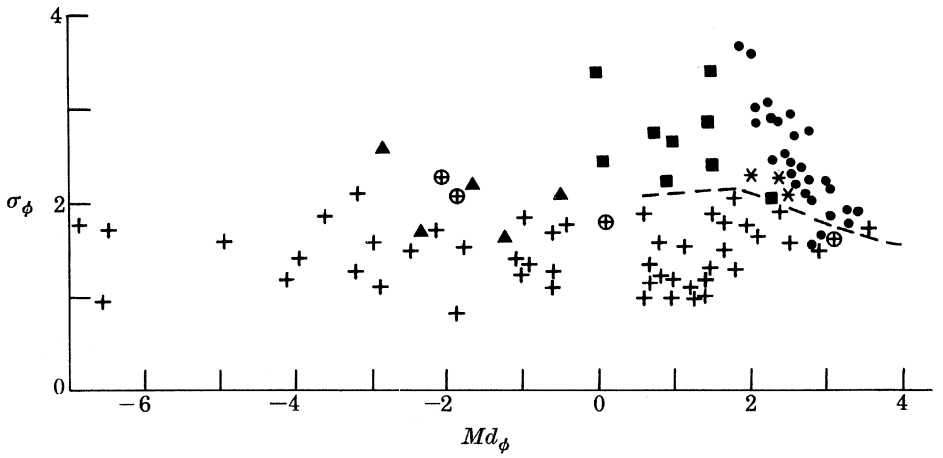

FIGURE 17. Median diameter (Md_ϕ) against sorting parameter (σ_ϕ) delineating main fields of Askja ejecta. +, Layer D; ■, layer C_2 (base surge deposits); ●, layer C_1: ▲, layer E; ⊕, layer B; ★ Viti phreatic rim deposits. The dashed line separates the fall and flow fields of Walker (1971).

Layer C shows downwind coarse-tail grading in which only the coarse particles are sorted. This is illustrated in figure 20*b*, where four frequency-size distributions are shown from 2 to 58 km downwind. The grain-size analyses are similar except for the gradual loss of a coarse-tail fraction downwind. The downwind sorting of coarse clasts is more easily recognized in the maximum grain-size isopleth (figure 15*b*). All grain-size fractions in C, except the coarsest, have been deposited from the rim of the vent to over 90 km from source. The decrease of σ_ϕ is due to removal of coarse clasts downwind.

Another contrast between layer D and layer C is the skewness of the size distribution (α_ϕ) which is distinguished on a plot of α_ϕ against σ_ϕ (figure 21). All but four of the layer-D samples are positively skewed, indicating an extended fine tail. The positive skewness is believed to be largely due to breakage generating a poorly sorted secondary mode which is superimposed on the main fall-out mode. Inevitably, positive skewness is partly due to artificial break-up during sieving. However, at least two natural processes lead to positive skewness. One is impact breakage, which occurs close to the source. Layer B shows large values of positive skewness (figure 21) which we attribute to substantial impact breakage. The second cause of positive skewness is premature fall-out of small clasts from an eruption column. Intense turbulent

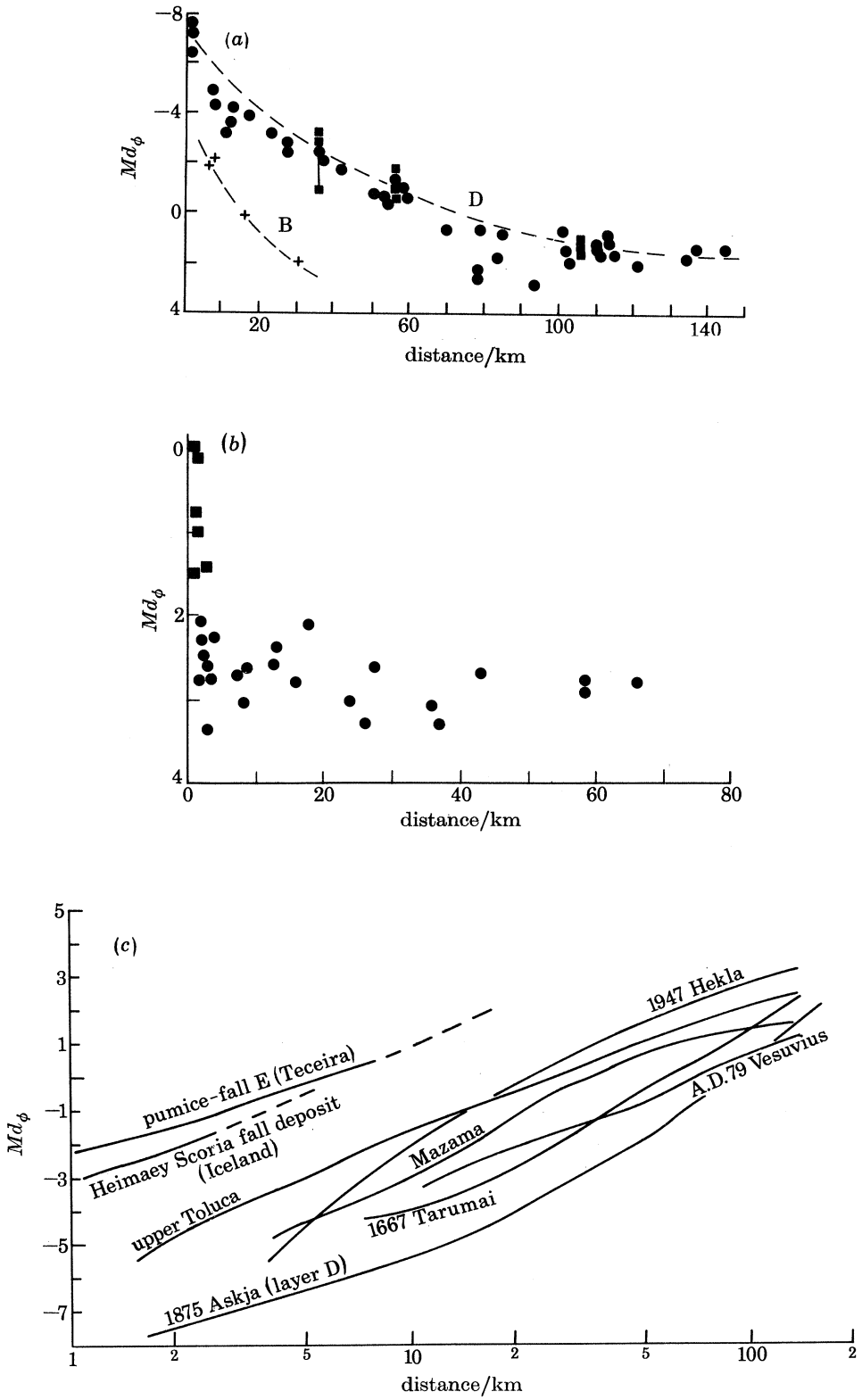

FIGURE 18. Median grain diameter (Md_ϕ) again distance for (*a*) layers B and D, and (*b*) layer C; (*c*) other pyroclastic fall deposits for comparison.

mixing with air at the sides of an eruption column inevitably leads to small clasts leaving the column at a much lower height than the average for that size, increasing the fine tail.

The negative skewness observed in all samples of layer C (figure 21) is due to an extended coarse tail and concentration of the bulk of ejecta in the fine-grain sizes (figure 20*b*). We interpret this as due to the mixing of two populations of grain size with different origins. One population is a broad spread of sizes from coarse to fine. The other is a well sorted population restricted to the fine-grain sizes.

Layer C has characteristics that are attributable to phreatomagmatic activity. The occurrence

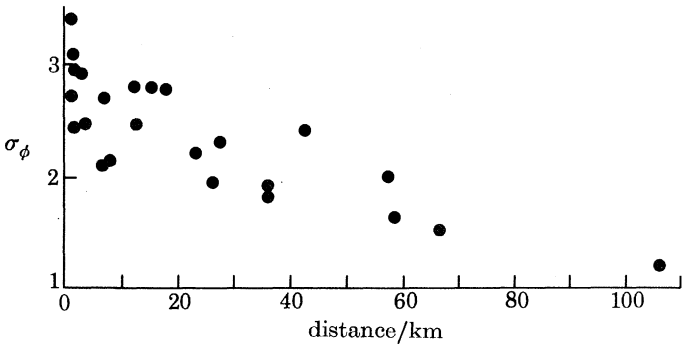

FIGURE 19. Sorting parameter (σ_ϕ) against distance from source for layer C.

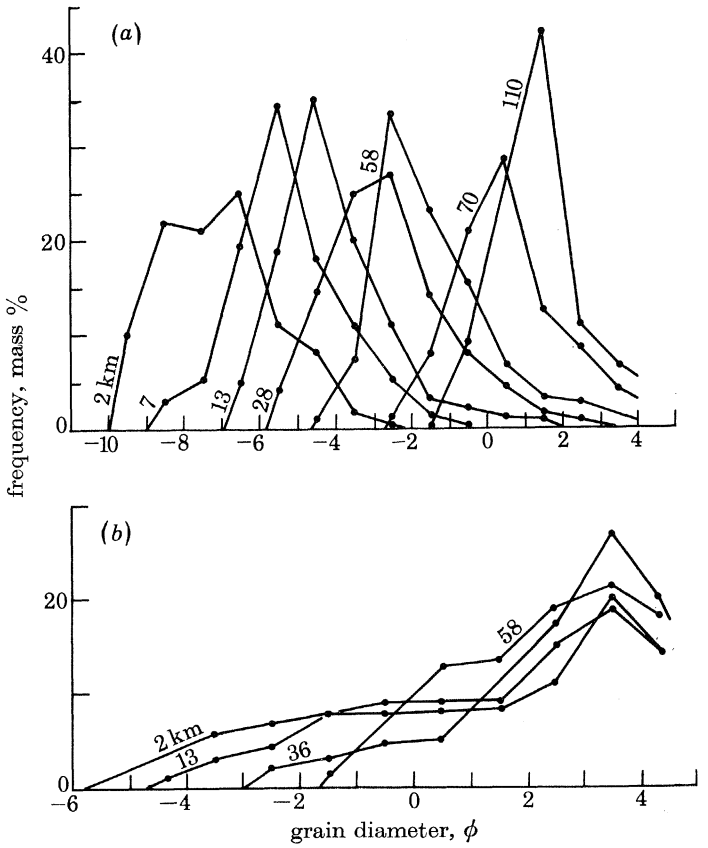

FIGURE 20. Frequency size curves are shown for layer D (*a*) and layer C (*b*) at various distances from source along the dispersal axis.

of base surge beds, the fine-grain size, even close to the source, the poor sorting and well stratified appearance all suggest an origin by phreatomagmatic explosions (Self & Sparks 1978). In basaltic eruptions the pyroclastic deposits from Surtseyan-type phreatomagmatic explosions show the same characteristics (Walker & Croasdale 1972). Surtseyan eruptions produce restricted dispersal to form tuff rings. The Askja activity was more powerful and formed a widespread sheet (layer C).

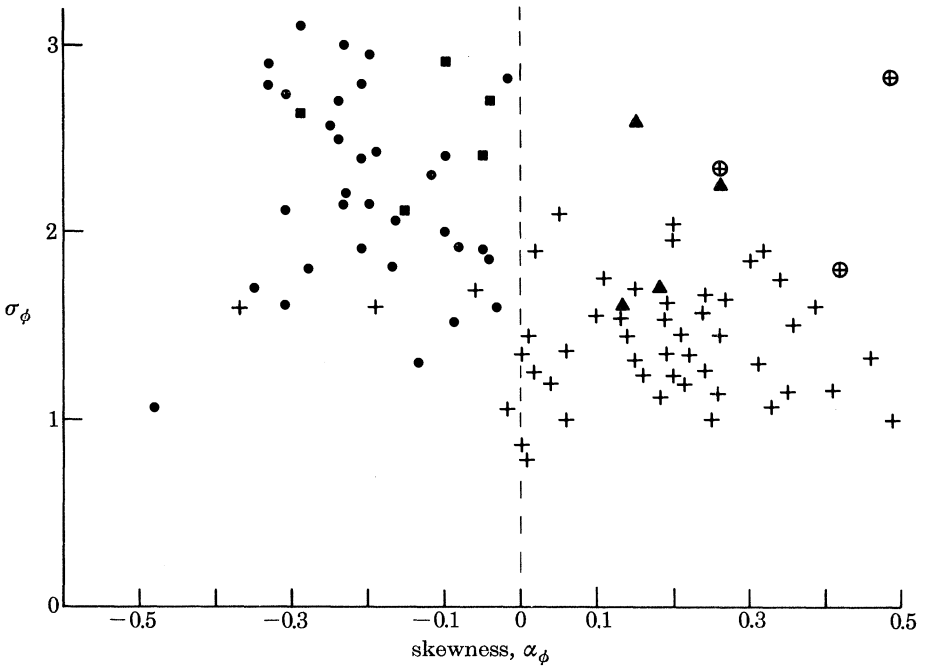

FIGURE 21. Sorting parameter (σ_ϕ) against skewness (α) for the principal tephra layers of the 1875 Askja eruption. The figure illustrates the contrasts between layers C and D in grain size distributions. Meaning of symbols as in figure 17.

The absence of downwind sorting of most particles and the deposition of fines even close to source is the main distinguishing feature of layer C. The wide dispersal of this layer and downwind coarse-tail grading suggest a high eruption column. The only way to inhibit downwind sorting of fines is by aggregation of the particles into clumps. We have found no accretionary lapilli, but suggest that poor sorting is a result of either rain flushing or condensation of water on to particles and aggregation of the wet particles. The source of the water is probably steam generated during the interaction of water and magma. During the 1979 phreatomagmatic explosions of Soufrière, St Vincent, accretionary lapilli were observed to fall and disintegrate on impact, forming a fine grained, poorly sorted ash-fall deposit like layer C with few lapilli preserved.

In figure 22 we plot the Askja deposits on a classification diagram proposed by Walker (1973), where the dispersal index (D) is plotted against a fragmentation index (F) defined as the percentage of sub-millimetre particles in a sample taken on the dispersal axis at the $0.1T_{max}$ isopach. Walker (1973) divides the diagram into several different classes of deposit. Magmatic explosive eruptions fall in a series: hawaiian; strombolian; sub-plinian; and plinian, with increasing dispersal in the series and relatively low fragmentation indices. Layer B plots in the

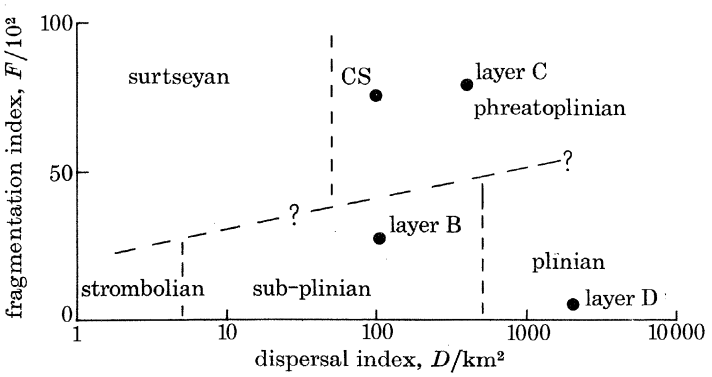

FIGURE 22. A fragmentation index (F) is plotted against a dispersal index (D) for the main Askja layers, after the classification scheme of Walker (1973). Definitions of D and F are given in the text.

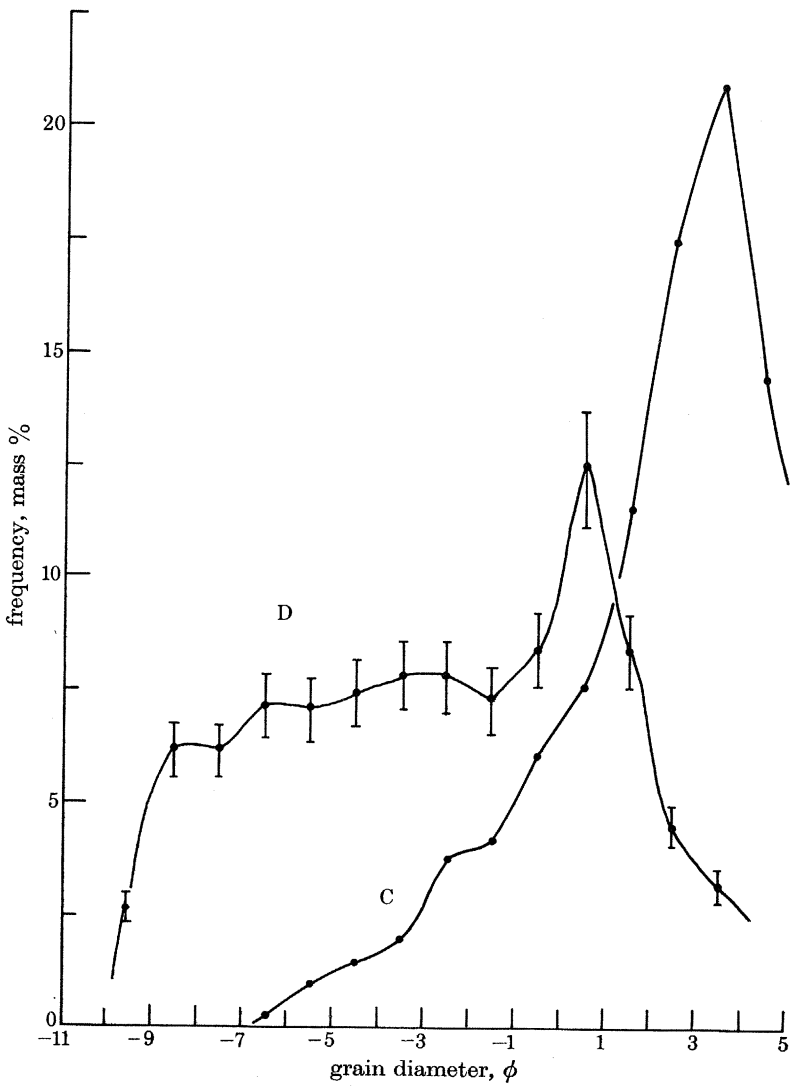

Figure 23. Total grain size distribution frequency curves of layers D and C on land.

sub-plinian field and layer D is clearly plinian. Surtseyan deposits plot with high values of F and low values of D.

Layer C plots with high D and high F. Silicic pyroclastic deposits with similar characteristics to layer C are in fact common. Walker (1973) documents the Caldeira Secca tephra layer on São Miguel which similarly has a high F-value and high D-value. Parts of the Minoan deposit of Santorini are of this type (Bond & Sparks 1976), and some of the rhyolitic tephra in the Taupo volcanic zone of New Zealand have such features (Self & Sparks 1978). Self & Sparks (1978) propose that such deposits be termed *phreatoplinian*, because the deposits have a wide plinian-style dispersal indicating a high eruption column, yet have all the other characteristics of phreatomagmatic deposits.

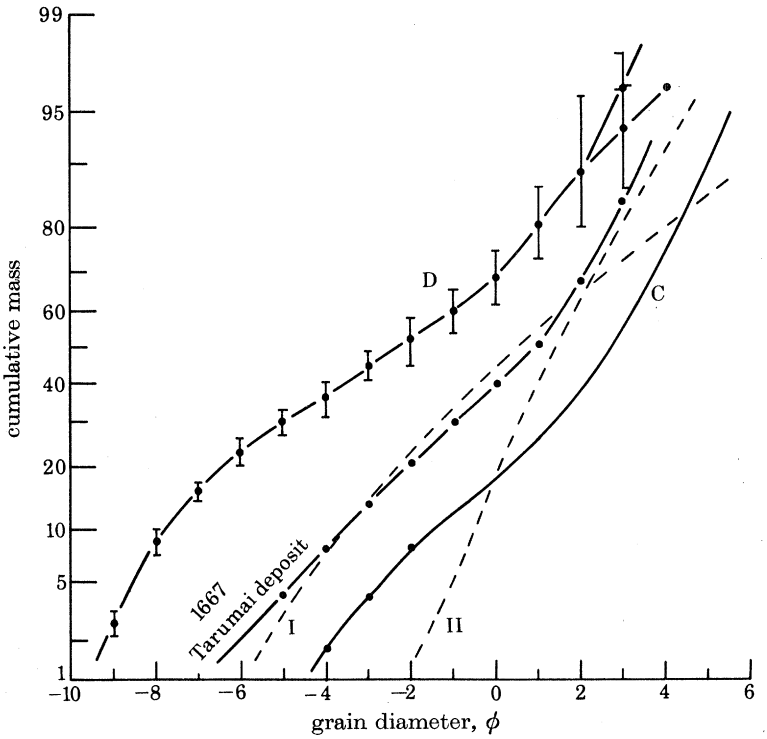

FIGURE 24. Cumulative frequency curves for the total grain size distributions of layers D and C on land. Data on the 1667 Tarumai pumice deposit after Suzuki *et al.* (1973) are shown for comparison. – – –, Distributions of the coarse (I) and fine modes (II) of layer C.

Recognition of this type of deposit develops Walker's classification scheme and demonstrates that there is a series of high F-value phreatomagmatic deposits analogous to the hawaiian-to-plinian series. At present Self & Sparks (1978) recognize only two types of category in this series: Surtseyan and phreatoplinian. The essential difference is that the former produces a tuff ring and the latter, being widely dispersed, does not. In figure 22 the division between the two types is arbitrarily at $D = 50$ km^2.

Total grain size distribution

The total grain size population of an individual pyroclastic deposit is an important parameter in studies of eruption mechanisms and in classifying pyroclastic deposits. There are, however,

considerable problems in estimating the total size-population. A major difficulty is that fine-grained distal ash is usually removed shortly after an eruption and thus accurate determinations are only feasible immediately after an eruption.

In Askja, the lack of downwind sorting in layer C makes an estimate comparatively accurate. Figure 23 shows an average mass % histogram of layer C. Two distinct grain-size populations occur: a broad coarse mode and a fine well-sorted population. The two populations are also distinguished in a cumulative frequency curve (figure 24), which is reflected in strong negative skew value (table 4). We have estimated the two individual populations by extrapolation. Both modes show normal distribution, reflected in near zero skewness. We interpret these populations as the result of two different styles of magma breakage.

TABLE 4

	Md_ϕ	σ_ϕ	α_ϕ
layer D	−2.3	4.25	−0.11
1667 Tarumai	+0.9	3.00	−0.17
layer C	+2.8	2.40	−0.29

For layer D we estimated the total size distribution by subdividing the isopach map (figure 10*a*) and averaging the grain-size analyses of all samples within 27 sub-units. We weighted the proportion of each grain-size class according to the volume within each sub-unit, and then calculated a total size distribution by integrating the data (table 3, analysis 12). The data are plotted as a size frequency curve (figure 23). Unexpectedly, the data show a pronounced peak in the 0–1 ϕ-values. The data in figure 23 apply only to the deposit on land. On the eastern coast of Iceland to 0–1 size fraction is the mode of the distribution, so that sizes less than $\frac{1}{2}$ mm are clearly under-represented as they were lost to sea.

Layer D apparently has a separate, fine grained, well sorted population corresponding to the same peak in layer C. Thus layer D is bimodal, which is reflected in a large value of negative skewness (table 4): this contrasts with the individual samples, which are all positively skewed (figure 21). A major difference between layer D and layer C is that in the former the coarse population dominates the distribution, whereas in layer C the fine population dominates the distribution. For example, layer D has a much larger value of σ_ϕ than layer *C* (table 4), despite the loss of part of the fine tail to sea.

Our data confirm that layer D is particularly coarse-grained. The 1667 Tarumai pumice deposit, Japan (Suzuki *et al.* 1973) is shown for comparison (figure 36 and table 4). The Tarumai data are also for the whole deposit up to 150 km from source. The Tarumai deposit has much smaller values of Md_ϕ and σ_ϕ. However, it is evident from the data of Suzuki *et al.* that there may also be a similar bimodality to layer D, as shown in negative skew values. As with layer D, nearly all individual samples of this deposit are positively skewed.

The total grain-size populations are interpreted as being mainly reflexions of processes of magma fragmentation. We suggest that the primary fragmentation process in layer D is the expansion of decompressing magmatic gas. The second fine-grained population is then believed to be generated by secondary fragmentation processes such as attrition and impact of particles in the conduit, where the concentration of particles is sufficiently high that particle-to-particle collisions and collisions with the vent wall are common.

PHILOSOPHICAL TRANSACTIONS OF THE ROYAL SOCIETY A MATHEMATICAL, PHYSICAL & ENGINEERING SCIENCES

In layer C the fine population dominates the deposit. Here we suggest that the interaction of water with the disrupting magma results in a second, intense fragmentation leading to a much finer grained total population of particles, and a high proportion of fine particles. The two fine peaks in both deposits may represent a barrier for all fragmentation processes. Particles finer than $\frac{1}{2}$ mm may be much stronger than coarser pumice clasts, resulting in concentration in these grain sizes and inhibiting production of even finer grain-sizes.

TABLE 5. MODAL PROPORTIONS OF LITHIC COMPONENTS

	obsidian (%)	granite (%)	basalt (%)
layer D	37	12	51
layer E	45	14	41

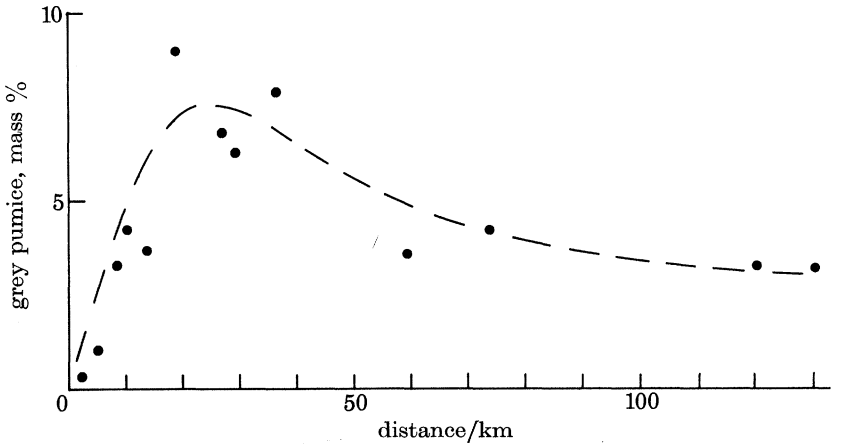

FIGURE 25. The mass percentage of grey mixed pumice clasts in layer D against distance from source.

Component analyses

Samples of layer D were analysed by separating and weighing the main components in each size clast (Table 5). There is a systematic initial increase in the mass percentage of grey mixed pumices along the dispersal axis in layer D (figure 25) and then a subsequent decrease beyond 50 km. We have weighted the analyses to account for the approximate volume of the deposit represented by each analysis, and the total mass percentage of mixed pumice in layer *D* is estimated as 4.7. The concentration of grey pumice clasts in the 15–50 km range is attributed to the small characteristic size of the grey pumice. The two magma types were intimately mixed prior to eruption (Sparks *et al.* 1977), and the contaminated rhyolite has a characteristic size between 1 and 0.1 cm. These sizes, and thus the grey pumice, were largely accumulated in the 15–50 km distance range. The mixing of basaltic and rhyolitic magmas is so intimate and variable that we adopted the strategy of analysing chemically the separated grey pumices to assess the relative proportions. Table 1 (analysis 11) gives the average of four such analyses, which indicates that the mixed pumices contain on average 40 % basaltic glass, implying that the total mass percentage of basaltic magma was only 1.9.

The proportion of lithic clasts ranged from 0.4 to 4.1 % and averaged 2.1 % in layer D. This is low compared to many other plinian deposits: for example, the A.D. 79 Pompeii and Avellino

deposits contain between 7 and 20% lithics (Lirer *et al.* 1973). Although the proportion of lithics is small, the total volume is 6.3×10^6 m^3, which would represent a hypothetical cored-out cylindrical conduit 50 m in radius and 800 m deep, or 100 m in radius and 200 m deep.

Ejecta density and shape

Each pumice clast was treated as an ellipsoid, and the three mutually normal axes X, Y and Z, which are the major, intermediate and minor axes, were measured. Axial ratios vary considerably, and table 6 shows the mean axial ratios and standard deviation from the mean. We tested the assumption of ellipsoidal shape by a photogrammetric method to determine the volumes of 23 pumice clasts in the laboratory (Blackburn 1977). The method consists of photographing each clast along its three principal axes, measuring the projected shape of each frame and numerically integrating the data in three dimensions to obtain a volume. The volume of a pumice clast can be expressed as

$$\text{volume} = K(XYZ),$$

TABLE 6. DATA ON PUMICE AXIAL RATIOS

axis ratio	mean	standard deviation from mean	no. of samples
X/Y	1.57	1.43	610
Y/X	1.87	0.71	607
X/Z	2.89	1.34	612

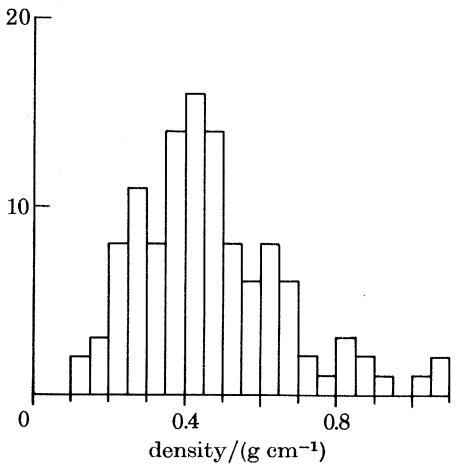

FIGURE 26. Histogram of pumice densities in proximal localities of layer D.

where K is a constant. If the body is an ellipsoid then $K = \frac{4}{3}$. For 23 samples K had a mean value 3.25, with individual determinations ranging from 2.67 to 4.07. The wide range of values of K shows that field determinations of volume are not very precise (20% error). Densities were determined from volume and field weight measurements by using $K = 3.25$.

Figure 26 shows a histogram of 116 field density-determinations on pumice fragments, all exceeding 32 mm in size, from the plinian layer D deposit at the eastern edge of Oskjuvatn (the same locality as sieve analysis 1, table 3). The mean density of the pumice clasts is 0.44 g/cm^3 with a standard deviation of 0.19 g/cm^3.

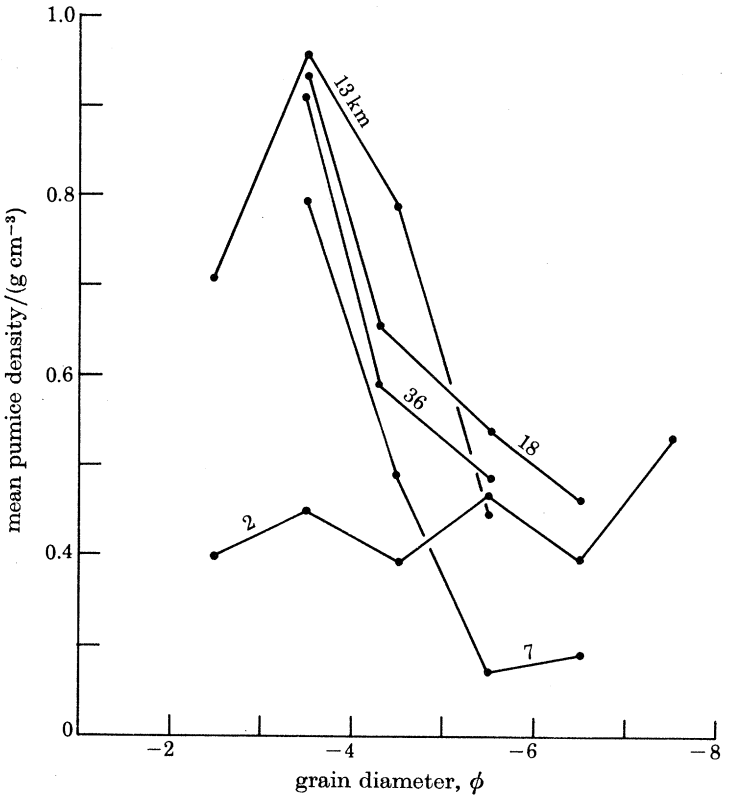

FIGURE 27. The relation between clast density and grain diameter is illustrated for samples of layer D at various distances from the source.

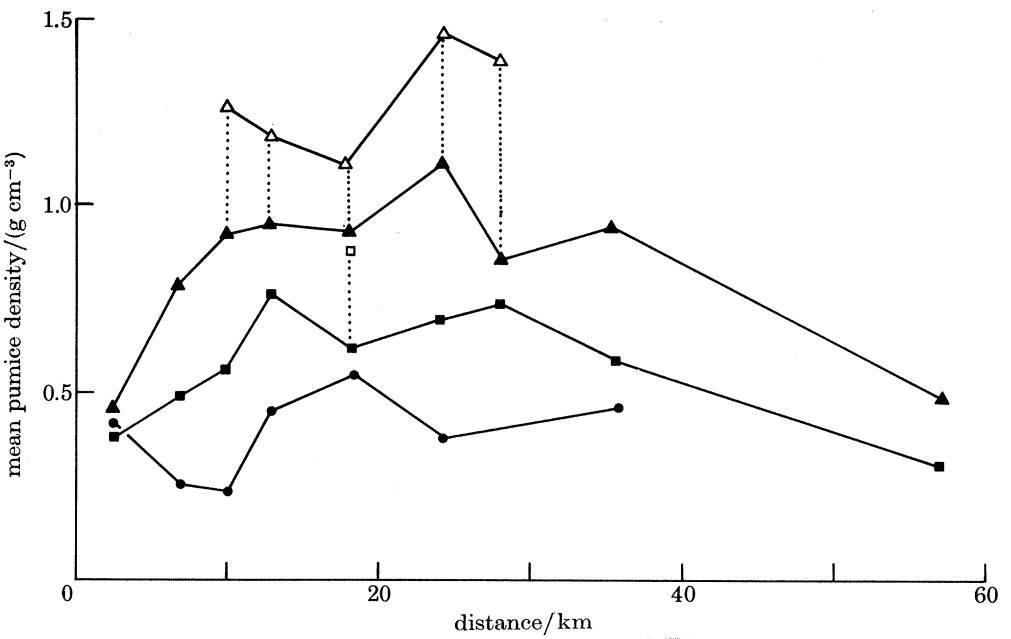

FIGURE 28. Density against distance for individual size classes in layer D. ●, 32–16 mm size range; ■, 16–8 mm size range; ▲, 8–4 mm size range; □ and △, grey pumice clasts.

PHILOSOPHICAL TRANSACTIONS OF THE ROYAL SOCIETY A MATHEMATICAL, PHYSICAL & ENGINEERING SCIENCES

Figure 27 also shows the variation of density with size in several samples of the plinian layer at various distances along the dispersal axis. In all but one of these samples there is a systematic increase in density with decreasing grain size. This feature is typical of plinian pumice deposits (Lirer *et al.* 1973; Walker 1971), owing to æolian fractionation. Figure 27 also shows the mean density of each grain-size clast taken from a locality on the rim of Oskjuvatn. Here there is no significant correlation between size and density. We interpret this as due to the smaller grain sizes at this near-source location being almost entirely formed by impact breakage of large pumice clasts. Where impact breakage is significant, the smaller clasts would have the same density as the coarser parent pumices. The lack of grey pumices in the 0.4–1.6 cm size clasts at this same location is due to a lack of primary pumice in the coarser fraction.

Figure 28 gives the mean pumice density in the three size classes from 0.8 to 6.4 cm against distance from the vent. All the data except for the 0.8–1.6 cm size fraction relate to white pumice only. Each size class shows a broad maximum in density. We interpret the variations as being due to the effect of impact breakage at distances less than 10 km, where these grain classes make up the fine tail. As impact breakage becomes less important in generating the fine tail, the density increases. Beyond the broad maximum the density falls in a given size fraction by wind sorting (the denser clasts falling out earlier).

Conclusions

The 1875 eruption of Askja is one of the youngest examples of a rhyolitic plinian eruption. The excellent preservation of the deposits and the historical observations have allowed us to document the eruption and its products in unusual detail. The data presented are relevant both to the circumstances of rhyolitic volcanism in Iceland and to the interpretation of plinian pyroclastic deposits.

The volcanic and tectonic events, which took place in the northeastern rift zone of Iceland in 1874 and 1875, involved both the Askja central volcano and the associated fissure swarm, extending over 90 km to the north. One consequence of this episode of crustal rifting was the movement of ferrobasalt from a reservoir beneath Askja along the fissure swarm to the eruptive fissure at Sveinagja (Sigurdsson & Sparks 1978*a*, *b*). Detailed petrological studies (Sigurdsson & Sparks, in the press) also indicate that primitive tholeiitic magma influxed into the magma chamber beneath Askja, resulting in a complex sequence of mixing events between the primitive basalt, ferrobasalt and rhyolite and culminating in the 1875 explosive eruption (Sparks *et al.* 1977). These observations and interpretations indicate a major causative role for basalt in controlling the occurrence of rhyolite volcanism in Iceland during periods of major tectonic activity.

The pyroclastic deposits have a total volume of 0.2 km^3 of dense rhyolitic magma which only represents 10% of the volume of Oskjuvatn caldera. We conclude that the caldera formed, in a piecemeal fashion, by withdrawal of magma from the reservoir beneath Askja, rather than as the result of the explosive discharge of large volumes of rhyolitic magma. The large calderas of Iceland, associated with both basaltic and rhyolitic volcanism, are thus dominantly of Kilauean type (see Sigurdsson & Sparks 1978*a* for evidence on basaltic calderas). Thickness and maximum grain-size data also show that the vents were on a north–south line, 1.5 km long, and that the vent location moved north with time. We suspect that this line represents the ring fracture of the prehistoric caldera. The Viti crater was not the vent for the pumice eruption, but was formed by phreatic explosions after the March eruption.

PHILOSOPHICAL TRANSACTIONS OF THE ROYAL SOCIETY A MATHEMATICAL, PHYSICAL & ENGINEERING SCIENCES

The 1875 pyroclastic deposits are typical in many respects of the products of plinian activity. Layers B and D have coarse grain size and wide dispersal together with reverse grading, low lithic contents, and poor development of internal stratification. Although widely dispersed, layer C has characteristics which are satisfactorily interpreted as the consequence of phreatomagmatic activity: fine grain size near source, poor sorting, well-developed stratification and base surge bed-forms. Access of water to a vent during plinian activity greatly increases fragmentation of the magma, and an additional type of deposit, phreatoplinian, can be added to the classification scheme of Walker (1973), exemplified by layer C.

The depositional processes in layers D and C were fundamentally different, as reflected in the contrasting downwind grain size variation in the deposits. Layer D, in common with other plinian layers, shows downwind distribution grading characterized by a decrease in Md_ϕ and no change in σ_ϕ. Layer C shows little change in Md_ϕ downwind, but shows a decrease in maximum grain size and σ_ϕ. This feature of coarse-tail grading is interpreted as being due to aggregation of wet particles in a stream-rich eruption column, and is clearly a characteristic of phreatomagmatic activity (Self & Sparks 1978). Another important consequence of downwind is the concentration of grey mixed pumice clasts at distances of 15–50 km from Askja in layer D. This is a hydraulic effect, and illustrates that the proportions of components in a pyroclastic deposit can only be accurately determined by regional mapping.

Another contrast between layers C and D is evident in the total grain size distribution of each deposit, reflecting the different styles of explosive activity which produced them. Layer D is relative coarse-grained, although at least 55% of the ejecta is finer than 1 mm. The main mechanism of magma fragmentation is considered to be by expansion of exsolving gases, although the fine mode in the sub-millimetre size fractions suggests a second fragmentation process. Layer C is much finer over all (90% less than 1 mm) and displays strong bimodality with a dominant fine mode. The bimodality is interpreted as a consequence of two fragmentation processes: initial disruption of magma by gases followed by intense fragmentation of these pieces by explosive interaction with water.

An important observation recorded in the field and evident in the density data is that impact breakage is a major controlling process affecting grain size distribution near source. Substantial impact breakage is evident in clasts greater than 10 cm in diameter. The effect of this breakage, together with the sampling problems associated with maximum grain size near source, suggests that eruption parameters such as gas velocity will tend to be underestimated in prehistoric plinian deposits.

The Askja plinian deposits show increasing dispersal with time as measured by Walker's dispersal index, and overall reverse grading of the maximum pumice diameter. Both these observations are explained by increasing eruption column height, which can be directly related to increasing discharge rate of magma (Wilson *et al.* 1978). The most pronounced reverse grading occurs at distances between 20 and 80 km in layer D, which generally consists of clasts greater than 10 cm in diameter. The northerly dispersal of large pumice clasts in layer D near source also contrasts with the easterly wind-condtrolled dispersal of clasts smaller than 40 cm.

These observations can be interpreted in terms of the model for plinian eruption columns presented by Wilson *et al.* (1980). The dispersal of large pumice clasts is controlled by the gas exist velocity in the vent, and the angle of ejection. Large clasts leave the column at a low level and are not strongly affected by the wind. Grading in large clasts is independent of eruption column height. Wilson *et al.* (1980) have shown that gas exit velocity is strongly influenced by

magma gas content. The lack of near-source grading is interpreted as evidence of reasonably steady gas content in the magma. Model calculations suggest exit velocities averaged 380 m/s ($\pm$ 20 m/s) during the formation of layer D, reflecting a magma gas content of 3 % if H_2O is the volatile phase. Reverse grading of smaller pumice clasts further downwind reflects increasing release height of clasts in the eruption column. This is interpreted as being due to increasing magma discharge rate (Wilson *et al.* 1980) resulting in a growing and more vigorous eruption column as the eruption progressed.

The Royal Society funded field work with additional support from the U.S. National Science Foundation (grant nos. EAR 76-22083 and EAR 76-22319). We declare our graditude to several Icelandic scientists whose breakthrough studies of the 1975–1978 Krafla events came at a fortuitous time for us. These scientists include Kristjan Saemundsson, Axel Bjornsson, Oddur Sigurdsson, Eysteinn Trygvasson and Karl Gronvold. We are indebted to Dr Gudmundur E. Sigvaldsson for his cooperation and guidance. We give special thanks to Professor Sigurdur Thorarinsson for his help in our studies. The works of Professor Thorarinsson and Dr G. P. L. Walker on Icelandic geology and on the fundamentals of pyroclastic studies were a major inspiration. Dr E. A. Blackburn is thanked for efforts in the field. R. S. J. Sparks acknowledges a Nato post-doctoral fellowship tenured at the University of Rhode Island. We thank the Icelandic Research Counctil (VISINDASJODUR) for permission to carry out this research in Iceland. Contribution no. 51, Dept. Earth Sciences, University of Cambridge.

References

Bjornsson, A., Saemundsson, K., Einarsson, P., Tryggvason, E. & Gronvold, K. 1977 *Nature, Lond.* **266**, 318–323.
Bjornsson, A., Johnsen, G., Sigurdsson, S., Thorbergsson, G. & Tryggvason, E. 1979 *J. geophys. Res.* **84**, 3029–3038.
Blackburn, E. A. 1977 Ph.D. Thesis, University of Lancaster.
Blackburn, E. A., Wilson, L. & Sparks, R. S. J. 1976 *J. geol. Soc. Lond.* **132**, 429–440.
Bloomfield, N., Sanchez Rubio, G. & Wilson, L. 1977 *Geol. Rdsch.* **66**, 120–136.
Bond, A. & Sparks, R. S. J. 1976 *J. geol. Soc. Lond.* **132**, 1–16.
Booth, B. 1973 *Proc. Geol. Ass.* **84** (3), 353–370.
Booth, B., Walker, G. P. L. & Croasdale, R. 1978 *Phil. Trans. R. Soc. Lond.* A **288**, 271–319.
Crowe, B. M. & Fisher, R. V. 1973 *Bull. geol. Soc. Am.* **84**, 663–682.
Fisher, R. V. 1964 *J. geophys. Res.* **69**, 341–355.
Fudali, R. F. & Melson, W. G. 1972 *Bull. Volcan.* **35** (2), 383–401.
Gudmundsson, F. 1972 Endurminingar Vikurtgafan, 323 pp. Bokafelagid, Reykjavik.
Inman, D. L. 1952 *J. sedim. Petrol.* **22**, 125–145.
Kittleman, L. R. 1973 *Bull. Geol. Soc. Am.* **84**, 2957–2980.
Lirer, L., Pescatore, T., Booth, B. & Walker, G. P. L. 1973 *Bull. Geol. Soc. Am.* **84**, 759–772.
Mohn, H. 1878 Askregnen den 29 de–30 te Marts, 1975. Forhandlonger; *Videnskabssilskabet*. Christiania aar 1877, no. 10, Christiania.
Moore, J. G. 1967 *Bull. Volcan.* **30**, 337–363.
Persson, C. 1967 *Geol. För. Stockh. Förh.* **88**, 500–519.
Saemundsson, K. 1974 *Bull. Geol. Soc. Am.* **85**, 494–505.
Schmincke, H. V., Fisher, R. V. & Waters, A. C. 1973 *Sedimentology* **20**, 553–574.
Self, S. 1976 *J. geol. Soc. Lond.* **132**, 645–666.
Self, S. & Sparks, R. S. J. 1978 *Bull. Volcan.* **41**, 196–212.
Self, S., Sparks, R. S. J., Booth, B. & Walker, G. P. L. 1974 *Geol. Mag.* **111**, 539–548.
Sigurdsson, H. 1977 *Nature, Lond.* **269**, 25–28.
Sigurdsson, H. & Sparks, R. S. J. 1978*a* *Nature, Lond.* **274**, 126–130.
Sigurdsson, H. & Sparks, R. S. J. 1978*b* *Bull. Vulcan.* **41**, 149–167.
Sigurdsson, H. & Sparks, R. S. J. 1981 *J. Petrol.* (in press).
Sigvaldason, G. E. 1964 *Beitr. Miner. Petrogr.* **10**, 263–274.
Sigvaldason, G. E. 1968 *Contr. Miner. Petr.* **18**, 1–16.

PHILOSOPHICAL TRANSACTIONS OF THE ROYAL SOCIETY A MATHEMATICAL, PHYSICAL & ENGINEERING SCIENCES

Sparks, R. S. J. 1978 *J. Volcan. geothermal Res.* **3**, 1–37.
Sparks, R. S. J. & Wright, J. V. 1979 *Geol. Soc. Am. spec. Pap. on ash-flow tuffs* (ed. W. Elston & C. Chapin), pp. 155–166.
Sparks, R. S. J., Sigurdsson, H. & Wilson, L. 1977 *Nature, Lond.* **267**, 315–318.
Suzuki, T., Katsui, Y. & Nakamura, T. 1973 *Bull. volcan. Soc. Japan* **18**, 47–63.
Thoroddsen, Th. 1925 *Mem. R. Acad. Sci., Denmark*, **9**, 458 pp.
Thorarinsson, S. 1944 *Geogr. Annlr.* **26**, 1–217.
Thorarinsson, S. 1954 The eruption of Hekla 1947–1948. II. The tephra fall from Hekla on March 29, 1947. *Soc. Sci. Islandica*, Reykjavik. **3**, 1–68.
Thorarinsson, S. 1963 Askja on fire. Reykjavik.
Thorarinsson, S. 1968 *Geol. Rdsch.* **57**, 705–718.
Thorarinsson, S. 1971 In *Acta 1st Int. Sci. Conf. on the Volcano Thera, Athens*, 1971, 213–236.
Tryggvason, E. 1973 *Bull. seism. Soc. Am.* **63**, 1327–1348.
Walker, G. P. L. 1960 *J. Geol.* **68**, 515–528.
Walker, G. P. L. 1971 *J. Geol.* **79**, 696–714.
Walker, G. P. L. 1973 *Geol. Rdsch.* **62**, 431–446.
Walker, G. P. L. 1975 *Eruptive mechanisms in Iceland. Geodynamics of Iceland and the North Atlantic area* (ed. L. Kristjansson), pp. 189–201. Reidel and Sons.
Walker, G. P. L. & Croasdale, R. *J. geol. Soc. Lond.* **127**, 17–55.
Walker, G. P. L. & Croasdale, R. 1972 *Bull. Volcan.* **35** (2), 303–317.
Waters, A. C. & Fisher, R. V. 1971 *J. geophys. Res.* **76**, 5596–5614.
Wilson, L. 1972 *Geophys. Jl R. astr. Soc.* **30**, 381–392.
Wilson, L. 1976 *Geophys. Jl. R. astr. Soc.* **45**, 543–556.
Wilson, L., Sparks, R. S. J. & Walker, G. P. L. 1980 *Geophys. Jl R. astr. Soc.* **63**, 117–148.

PHILOSOPHICAL TRANSACTIONS OF THE ROYAL SOCIETY A MATHEMATICAL, PHYSICAL & ENGINEERING SCIENCES

FIGURE 3. Oblique aerial photograph of the Askja central volcano looking to the north in winter. The large prehistoric caldera and 1875 caldera are clearly delineated. The rugged mountains to the east of Oskjuvatn are composed of palagonite tuffs, pillow lavas and pillow breccias (the Moberg formation). The table mountain, Herdubreid, is observed in the upper right corner. (Photography by O. Sigurdsson.)

PHILOSOPHICAL TRANSACTIONS OF THE ROYAL SOCIETY A MATHEMATICAL, PHYSICAL & ENGINEERING SCIENCES

FIGURE 6. Layers C and D are shown on the northwest rim of Oskjuvatn. The subdivision of layer C into two units is readily apparent here. The base surge climbing megaripple structures are observed in layer C_2. The zones of darkened pumices in layer D pass laterally into patches of welded tuff.

GURE 7. Layer C_2 on the eastern rim of Oskjuvatn showing well developed bedding, disconformities due to erosion by base surges and by melt-waters from snow. Contemporaneous faults are common in layer C.

GURE 8. Layers D and C 10 km east of Oskjuvatn at Drekagil. Layer C is thin here as the location is on the edge of the deposit off the dispersal axis. Layer D shows pronounced reverse grading.

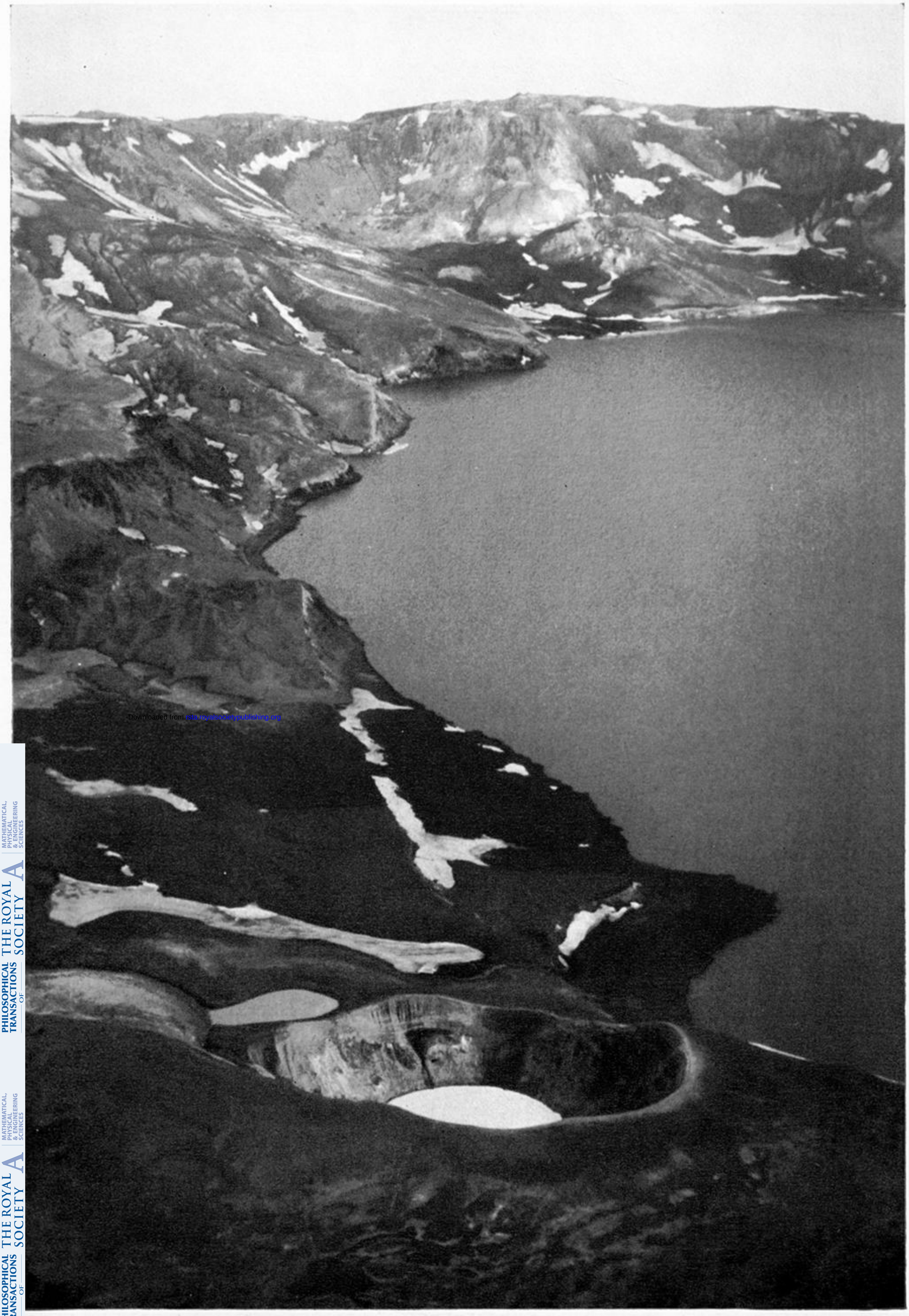

PHILOSOPHICAL TRANSACTIONS OF THE ROYAL SOCIETY A MATHEMATICAL, PHYSICAL & ENGINEERING SCIENCES

FIGURE 9. The Viti explosion crater and the northeastern edge of Lake Oskjuvatn. The 1924 aa lava flow is seen beyond Viti. (Photography by R. Greely.)